11

NUCLEAR REACTIONS

If energetic particles from a reactor or accelerator (or even from a radioactive source) are allowed to fall upon bulk matter, there is the possibility of a nuclear reaction taking place. The first such nuclear reactions were done in Rutherford's laboratory, using α particles from a radioactive source. In some of these early experiments, the α particles merely rebounded elastically from the target nuclei; this phenomenon, known ever since as Rutherford scattering, gave us the first evidence for the existence of atomic nuclei. In other experiments, Rutherford was able to observe a change or transmutation of nuclear species, as in this reaction done in 1919:

$$\alpha + {}^{14}\mathrm{N} \rightarrow {}^{17}\mathrm{O} + \mathrm{p}$$

The first particle accelerator capable of inducing nuclear reactions was built by Cockcroft and Walton, who in 1930 observed the reaction

$$\mathrm{p} + {}^{7}\mathrm{Li} \rightarrow {}^{4}\mathrm{He} + \alpha$$

In this chapter we discuss various types of nuclear reactions and their properties. In most cases, we deal with light projectiles, usually $A \leq 4$, incident on heavy targets; there is, however, much current interest in reactions induced by accelerating heavy ions (usually $A \leq 40$, but even beams as heavy as uranium are considered). We also deal only with reactions that are classified as "low energy," that is, of the order of 10 MeV per nucleon or less. In the range of 100 MeV–1 GeV, called "medium energy," meson production can take place, and protons and neutrons can transform into each other. At "high energy," all sorts of exotic particles can be produced, and we can even rearrange the quarks that are the constituents of nucleons. We discuss these latter types of reactions in Chapters 17 and 18.

11.1 TYPES OF REACTIONS AND CONSERVATION LAWS

A typical nuclear reaction is written

$$\mathrm{a} + \mathrm{X} \rightarrow \mathrm{Y} + \mathrm{b}$$

where a is the accelerated projectile, X is the target (usually stationary in the

laboratory), and Y and b are the reaction products. Usually, Y will be a heavy product that stops in the target and is not directly observed, while b is a light particle that can be detected and measured. Generally, a and b will be nucleons or light nuclei, but occasionally b will be a γ ray, in which case the reaction is called *radiative capture*. (If a is a γ ray, the reaction is called the *nuclear photoeffect*.)

An alternative and compact way of indicating the same reaction is

$$\mathrm{X(a,b)Y}$$

which is convenient because it gives us a natural way to refer to a general class of reactions with common properties, for example (α, n) or (n, γ) reactions.

We classify reactions in many ways. If the incident and outgoing particles are the same (and correspondingly X and Y are the same nucleus), it is a *scattering* process, *elastic* if Y and b are in their ground states and *inelastic* if Y or b is in an excited state (from which it will generally decay quickly by γ emission). Sometimes a and b are the same particle, but the reaction causes yet another nucleon to be ejected separately (so that there are three particles in the final state); this is called a *knockout* reaction. In a *transfer reaction*, one or two nucleons are transferred between projectile and target, such as an incoming deuteron turning into an outgoing proton or neutron, thereby adding one nucleon to the target X to form Y. Reactions can also be classified by the mechanism that governs the process. In *direct reactions* (of which transfer reactions are an important subgroup), only very few nucleons take part in the reaction, with the remaining nucleons of the target serving as passive spectators. Such reactions might insert or remove a single nucleon from a shell-model state and might therefore serve as ways to explore the shell structure of nuclei. Many excited states of Y can be reached in these reactions. The other extreme is the *compound nucleus* mechanism, in which the incoming and target nuclei merge briefly for a complete sharing of energy before the outgoing nucleon is ejected, somewhat like evaporation of a molecule from a hot liquid. Between these two extremes are the *resonance reactions*, in which the incoming particle forms a "quasibound" state before the outgoing particle is ejected.

Observables

We have at our disposal techniques for measuring the energies of the outgoing particles to high precision (perhaps 10 keV resolution with a magnetic spectrometer). We can determine the direction of emission of the outgoing particle, and observe its angular distribution (usually relative to the axis of the original beam) by counting the number emitted at various angles. The *differential cross section* is obtained from the probability to observe particle b with a certain energy and at a certain angle (θ, ϕ) with respect to the beam axis. Integrating the differential cross section over all angles, we get the total cross section for particle b to be emitted at a certain energy (which is also sometimes called a differential cross section). We can also integrate over all energies of b to get the absolute total cross section, which is in effect the probability to form nucleus Y in the reaction.

This quantity is of interest in, for instance, neutron activation or radioisotope production.

By doing *polarization* experiments, we can deduce the spin orientation of the product nucleus Y or perhaps the spin dependence of the reaction cross section. For these experiments we may need an incident beam of polarized particles, a target of polarized nuclei, and a spectrometer for analyzing the polarization of the outgoing particle b.

We can simultaneously observe the γ radiations or conversion electrons from the decay of excited states of Y. This is usually done in coincidence with the particle b to help us decide which excited states the radiations come from. We can also observe the angular distribution of the γ radiations, as an aid in interpreting the properties of the excited states, especially in deducing their spin-parity assignments.

Conservation Laws

In analyzing nuclear reactions, we apply the same conservation laws we applied in studying radioactive decays. *Conservation of total energy and linear momentum* can be used to relate the unknown but perhaps measurable energies of the products to the known and controllable energy of the projectile. We can thus use the measured energy of b to deduce the excitation energy of states of Y or the mass difference between X and Y. *Conservation of proton and neutron number* is a result of the low energy of the process, in which no meson formation or quark rearrangement take place. (The weak interaction is also negligible on the time scale of nuclear reactions, about 10^{-16} to 10^{-22} s.) At higher energies we still conserve total nucleon (or, as we discuss in Chapter 18, baryon) number, but at low energy we conserve *separately* proton number *and* neutron number. *Conservation of angular momentum* enables us to relate the spin assignments of the reacting particles and the orbital angular momentum carried by the outgoing particle, which can be deduced by measuring its angular distribution. We can thus deduce the spin assignments of nuclear states. *Conservation of parity* also applies; the net parity *before* the reaction must equal the net parity *after* the reaction. If we know the orbital angular momentum of the outgoing particle, we can use the $(-1)^\ell$ rule and the other known parities in the reaction to deduce unknown parities of excited states. In Section 11.3 we discuss yet another quantity that is conserved in nuclear reactions.

11.2 ENERGETICS OF NUCLEAR REACTIONS

Conservation of total relativistic energy in our basic reaction gives

$$m_X c^2 + T_X + m_a c^2 + T_a = m_Y c^2 + T_Y + m_b c^2 + T_b \qquad (11.1)$$

where the T's are kinetic energies (for which we can use the nonrelativistic approximation $\frac{1}{2}mv^2$ at low energy) and the m's are rest masses. We define the *reaction Q value*, in analogy with radioactive decay Q values, as the initial mass

energy minus the final mass energy:

$$\begin{aligned} Q &= (m_{\text{initial}} - m_{\text{final}})c^2 \\ &= (m_X + m_a - m_Y - m_b)c^2 \end{aligned} \qquad (11.2)$$

which is the same as the excess kinetic energy of the *final* products:

$$\begin{aligned} Q &= T_{\text{final}} - T_{\text{initial}} \\ &= T_Y + T_b - T_X - T_a \end{aligned} \qquad (11.3)$$

The Q value may be positive, negative, or zero. If $Q > 0$ ($m_{\text{initial}} > m_{\text{final}}$ or $T_{\text{final}} > T_{\text{initial}}$) the reaction is said to be *exoergic* or *exothermic*; in this case nuclear mass or binding energy is released as kinetic energy of the final products. When $Q < 0$ ($m_{\text{initial}} < m_{\text{final}}$ or $T_{\text{final}} < T_{\text{initial}}$) the reaction is *endoergic* or *endothermic*, and initial kinetic energy is converted into nuclear mass or binding energy. The changes in mass and energy must of course be related by the familiar expression from special relativity, $\Delta E = \Delta m c^2$—any change in the kinetic energy of the system of reacting particles must be balanced by an equal change in its rest energy.

Equations 11.1–11.3 are valid in any frame of reference in which we choose to work. Let's apply them first to the laboratory reference frame, in which the target nuclei are considered to be at rest (room-temperature thermal energies are negligible on the MeV scale of nuclear reactions). If we define a reaction plane by the direction of the incident beam and one of the outgoing particles, then conserving the component of momentum perpendicular to that plane shows immediately that the motion of the second outgoing particle must lie in the plane as well. Figure 11.1 shows the basic geometry in the reaction plane. Conserving linear momentum along and perpendicular to the beam direction gives

$$p_a = p_b \cos\theta + p_Y \cos\xi \qquad (11.4a)$$

$$0 = p_b \sin\theta - p_Y \sin\xi \qquad (11.4b)$$

Regarding Q as a known quantity and T_a (and therefore p_a) as a parameter that we control, Equations 11.3 and 11.4a, b represent three equations in four unknowns (θ, ξ, T_b, and T_Y) which have no unique solution. If, as is usually the case, we do not observe particle Y, we can eliminate ξ and T_Y from the equations

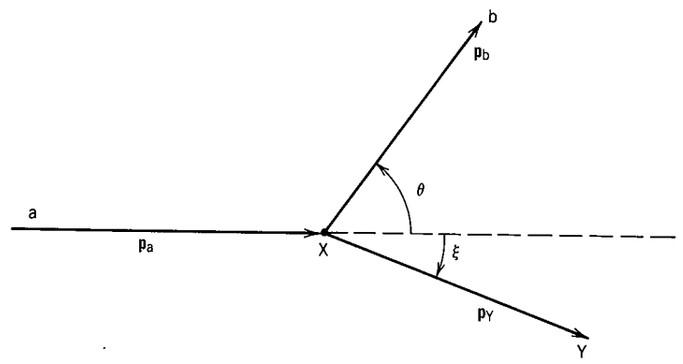

Figure 11.1 Basic reaction geometry for a + X → b + Y.

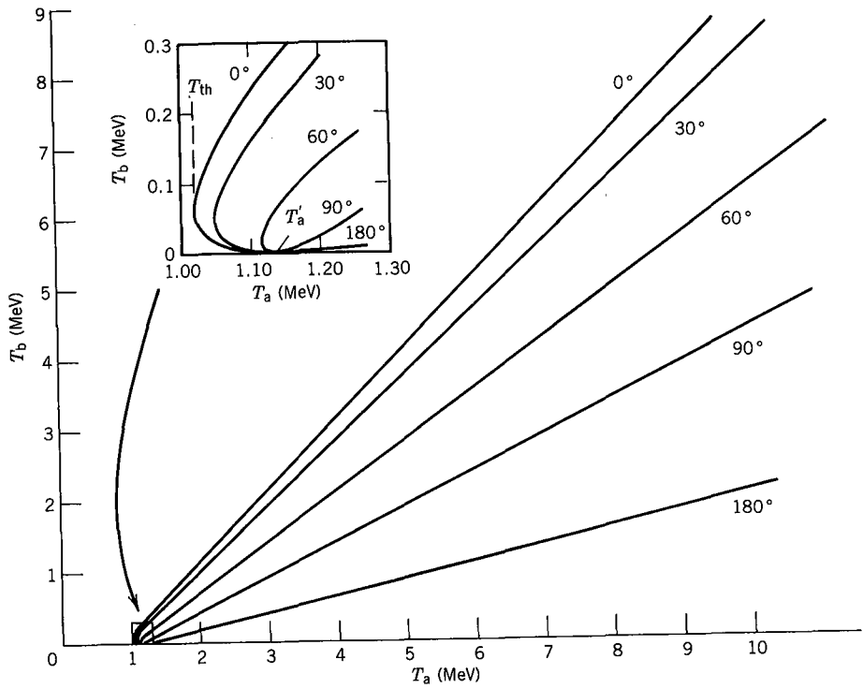

(a)

Figure 11.2 (*a*) T_a vs T_b for the reaction $^3H(p, n)^3He$. The inset shows the region of double-valued behavior near 1.0 MeV.

to find a relationship between T_b and θ:

$$T_b^{1/2} = \frac{(m_a m_b T_a)^{1/2} \cos\theta \pm \{m_a m_b T_a \cos^2\theta + (m_Y + m_b)[m_Y Q + (m_Y - m_a)T_a]\}^{1/2}}{m_Y + m_b} \tag{11.5}$$

This expression is plotted in Figure 11.2*a* for the reaction $^3H(p, n)^3He$, for which $Q = -763.75$ keV. Except for a very small energy region between 1.019 and 1.147 MeV, there is a one-to-one correspondence (for a given T_a) between T_b and θ. That is, keeping the incident energy fixed, choosing a value of θ to observe the outgoing particles automatically then selects their energy.

Several other features of Figure 11.2 are apparent, which you should be able to show explicitly from Equation 11.5:

1. There is an absolute minimum value of T_a below which the reaction is not possible. This occurs only for $Q < 0$ and is called the *threshold energy* T_{th}:

$$T_{th} = (-Q)\frac{m_Y + m_b}{m_Y + m_b - m_a} \tag{11.6}$$

The threshold condition always occurs for $\theta = 0°$ (and therefore $\xi = 0°$)—the products Y and b move in a common direction (but still as separate nuclei).

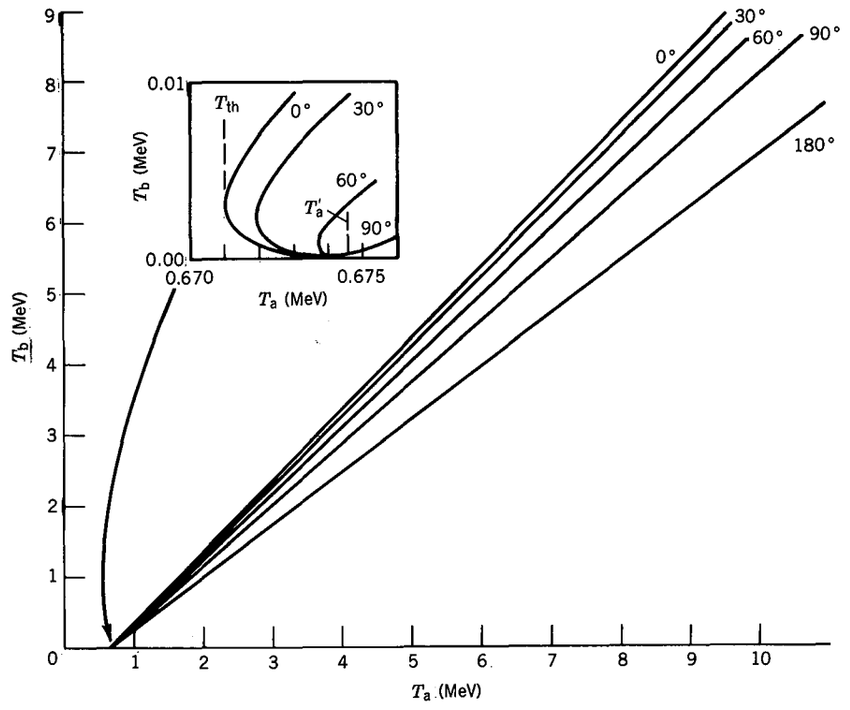

(b)

Figure 11.2 (*b*) T_a vs T_b for the reaction $^{14}C(p, n)^{14}N$. The inset shows the double-valued region.

No energy is "wasted" in giving them momentum transverse to the beam direction. If $Q > 0$, there is no threshold condition and the reaction will "go" even for very small energies, although we may have to contend with Coulomb barriers not considered here and which will tend to keep a and X outside the range of each other's nuclear force.

2. The double-valued situation occurs for incident energies between T_{th} and the upper limit

$$T'_a = (-Q)\frac{m_Y}{m_Y - m_a} \tag{11.7}$$

This also occurs only for $Q < 0$, and is important only for reactions involving nuclei of comparable masses. Using Equations 11.6 and 11.7 we can approximate this range as

$$T'_a - T_{th} \cong T_{th}\frac{m_a m_b}{m_Y(m_Y - m_a)}\left(1 - \frac{m_b}{m_Y} + \cdots\right) \tag{11.8}$$

and you can see that if a and b have mass numbers of 4 or less and if Y is a medium or heavy nucleus, then the range $(T'_a - T_{th})$ becomes much smaller

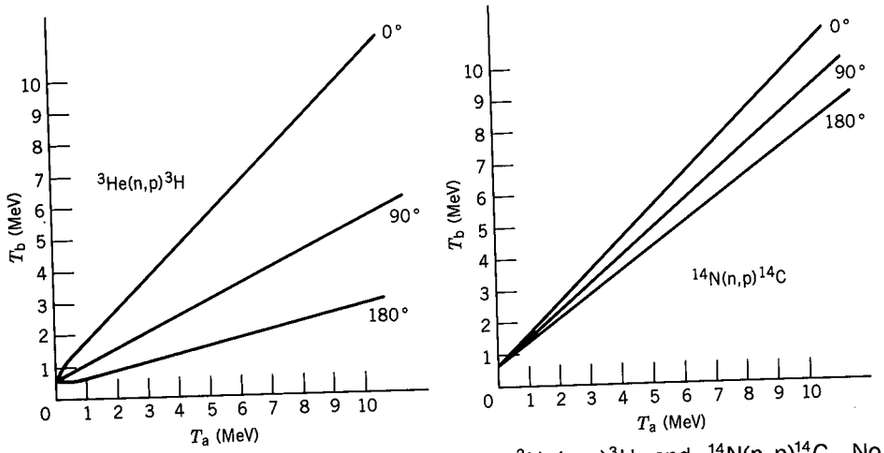

Figure 11.3 T_a vs T_b for the reactions ^{3}He(n, p)^{3}H and ^{14}N(n, p)^{14}C. No double-valued behavior occurs.

than 1% of the threshold energy. Figure 11.2*b* shows the double-valued region for the reaction ^{14}C(p, n)^{14}N.

3. There is also a maximum angle θ_m at which this double-valued behavior occurs, the value for which is determined for T_a in the permitted range by the vanishing of the argument in the square root of Equation 11.5:

$$\cos^2\theta_m = -\frac{(m_Y + m_b)[m_Y Q + (m_Y - m_a)T_a]}{m_a m_b T_a} \qquad (11.9)$$

When $T_a = T_a'$, the double-valued behavior occurs between $\theta = 0°$ and $\theta_m = 90°$; near $T_a = T_{th}$ it occurs only near $\theta_m = 0°$.

4. Reactions with $Q > 0$ have neither a threshold nor a double-valued behavior, as you can see by reversing the reactions shown in Figures 11.2*a* and 11.2*b*, ^{3}He(n, p)^{3}H and ^{14}N(n, p)^{14}C, for which we can in each case make the single transformation $-Q \rightarrow +Q$. Figure 11.3 shows the T_b vs T_a graphs for these cases. The reactions occur down to $T_a \rightarrow 0$ (no threshold), and the curves are single-valued for all θ and T_a.

If, for a given θ and T_a, we measure T_b, then we can determine the Q value of the reaction and deduce the mass relationships among the constituents. If we know m_a, m_b, and m_X, we then have a way of determining the mass of Y. Solving Equation 11.5 for Q, we obtain

$$Q = T_b\left(1 + \frac{m_b}{m_Y}\right) - T_a\left(1 - \frac{m_a}{m_Y}\right) - 2\left(\frac{m_a}{m_Y}\frac{m_b}{m_Y}T_aT_b\right)^{1/2}\cos\theta \qquad (11.10)$$

This procedure is not strictly valid, for m_Y also appears on the right side of the equation, but it is usually of sufficient accuracy to replace the masses with the integer mass numbers, especially if we measure at 90° where the last term vanishes.

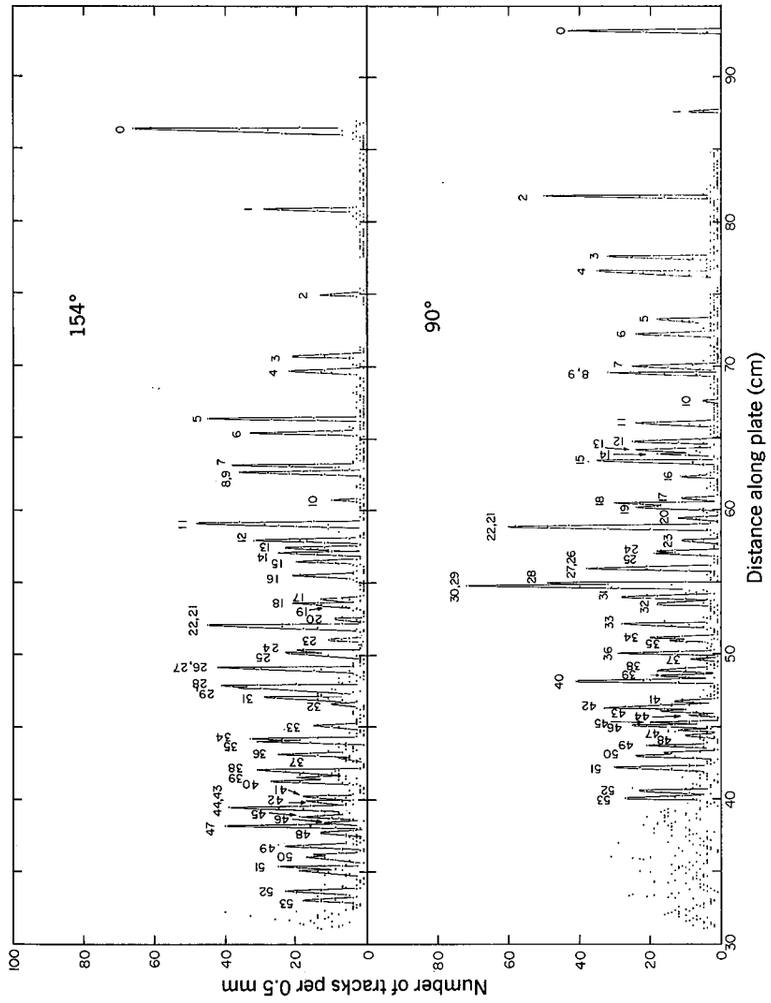

Figure 11.4 (*a*) Spectrum of protons from the reaction ^{58}Ni(^{4}He, p)^{61}Cu. The highest energy proton group populates the ground state of ^{61}Cu, while the remaining groups lead to excited states (numbered 1, 2, 3, ...). The spectra taken at angles of 90 and 154° show a very dramatic angular dependence; note especially the change in the cross section for groups 1 and 2 at the two angles. (*b*) γ rays following the reaction. (Data from E. J. Hoffman, D. G. Sarantites, and N.-H. Lu, *Nucl. Phys.* **A173**, 146 (1971).

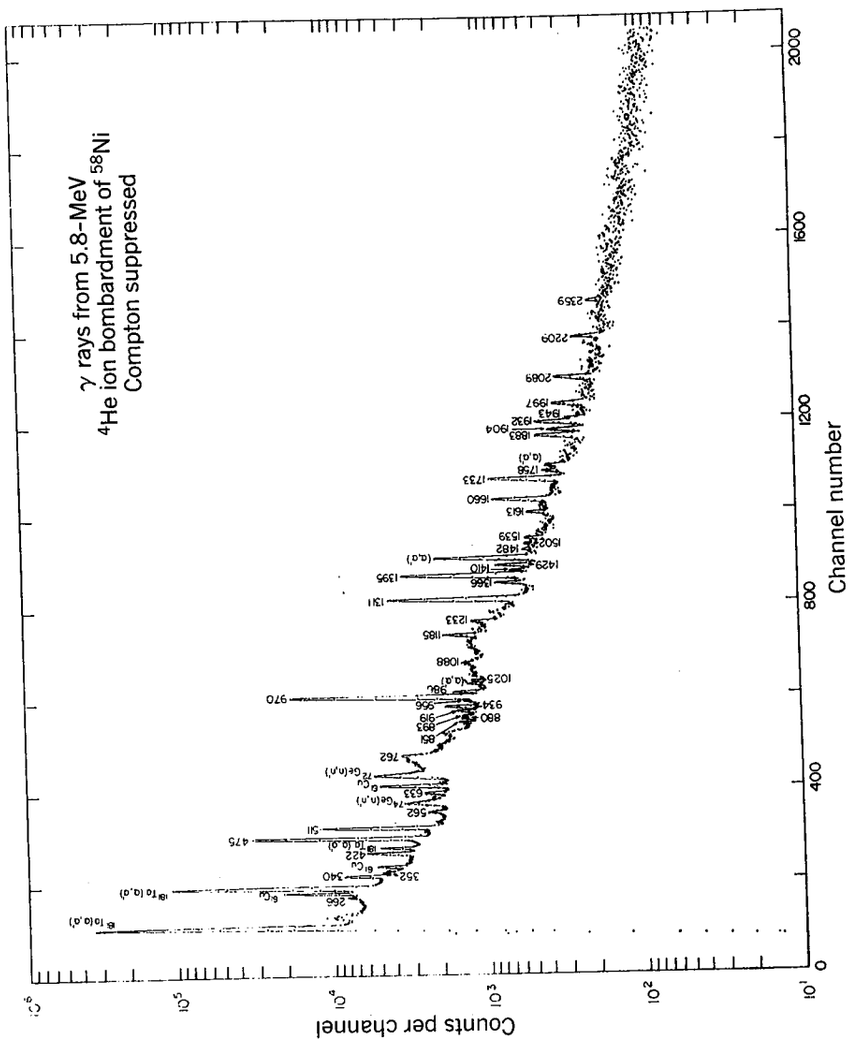

Figure 11.4 Continued. (*b*)

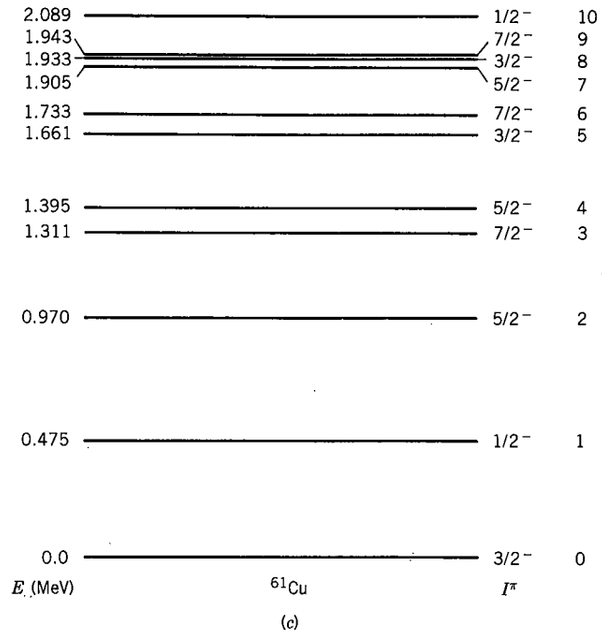

(*c*)

Figure 11.4 Continued.

As an example of the application of this technique, we consider the reaction $^{26}\text{Mg}(^{7}\text{Li}, ^{8}\text{B})^{25}\text{Ne}$. The nucleus ^{26}Mg already has a neutron excess, and the removal of two additional protons in the reaction results in the final nucleus ^{25}Ne with a large excess of neutrons. Data reported by Wilcox et al., *Phys. Rev. Lett.* **30**, 866 (1973), show a ^{8}B peak about 55.8 MeV observed at a lab angle of 10° when the incident ^{7}Li beam energy is 78.9 MeV. Using Equation 11.10 with mass numbers instead of masses gives $Q = -22.27$ MeV, which gives 24.99790 u for the mass of ^{25}Ne. Iterating the calculation a second time with the actual masses instead of the mass numbers does not change the result even at this level of precision.

If the reaction reaches excited states of Y, the Q-value equation should include the mass energy of the excited state.

$$\begin{aligned} Q_{\text{ex}} &= (m_{\text{X}} + m_{\text{a}} - m_{\text{Y}}^{*} - m_{\text{b}})c^2 \\ &= Q_0 - E_{\text{ex}} \end{aligned} \tag{11.11}$$

where Q_0 is the Q value corresponding to the ground state of Y, and where we have used $m_{\text{Y}}^{*}c^2 = m_{\text{Y}}c^2 + E_{\text{ex}}$ as the mass energy of the excited state (E_{ex} is the excitation energy above the ground state). The largest observed value of T_{b} is normally for reactions leading to the ground state, and we can thus use Equation 11.10 to find Q_0. Successively smaller values of T_{b} correspond to higher excited states, and by measuring T_{b} we can deduce Q_{ex} and the excitation energy E_{ex}.

Figure 11.4 shows an example of this kind of measurement. The peaks in the figure serve to determine T_{b}, from which the following Q values and excited-state

energies are obtained (energy uncertainties are about ± 0.005 MeV):

Peak	Q (MeV)	E_{ex} (MeV)
0	3.152	0.0
1	3.631	0.479
2	4.122	0.970
3	4.464	1.312
4	4.547	1.395
5	4.810	1.658
6	4.884	1.732
7	5.061	1.919
8, 9	5.090	1.938
10	5.240	2.088

leading to the excited states shown in the figure. The spectrum of the γ rays emitted following the reaction is also shown in the figure, and transitions can be seen corresponding to each of the deduced values of E_{ex} and therefore interpreted as direct transitions from the excited state to the ground state. Finally, angular distribution studies following the reaction can be used to deduce the spin-parity assignments of the excited states, leading to the level scheme shown in the figure. Notice how the various bits of data complement and supplement one another in building up the level scheme; from the γ rays alone, for example, we cannot tell which transitions connect the ground state with an excited state and therefore what the energies are of the excited states. The proton spectrum, however, gives us the excited-state energies directly, and turning to the γ-ray energies, which can be measured with greater precision, we can obtain more precise values for the energies of the states.

11.3 ISOSPIN

The interactions of a nucleon with its surroundings (other nucleons, for instance) in most cases do not depend on whether the nucleon has spin components $m_s = +\frac{1}{2}$ or $m_s = -\frac{1}{2}$ relative to an arbitrarily chosen z axis. That is, there is no need to distinguish in the formalism of nuclear physics between a "spin-up" nucleon and a "spin-down" nucleon. The multiplicity of spin orientations (two, for a single nucleon) may enter into the equations, for example in the statistics of the interaction, but the actual value of the projection does not appear. The exception to this situation comes about when a magnetic field is applied; the magnetic interaction of a nucleon depends on its spin component relative to the direction of the external field.

The charge independence of nuclear forces means that in most instances we do not need to distinguish in the formalism between neutrons and protons, and this leads us to group them together as members of a common family, the nucleons. The formalism for nuclear interactions may depend on the multiplicity of nucleon states (two) but it is independent of whether the nucleons are protons or

neutrons. The exception, of course, is the electromagnetic interaction, which can distinguish between protons and neutrons; with respect to the strong nuclear force alone, the symmetry between neutrons and protons remains valid.

This two-state degeneracy leads naturally to a formalism analogous to that of the magnetic interaction of a spin-$\frac{1}{2}$ particle. The neutron and proton are treated as two different states of a single particle, the nucleon. The nucleon is assigned a fictitious spin vector, called the *isospin*.* The two degenerate nuclear states of the nucleon in the absence of electromagnetic fields, like the two degenerate spin states of a nucleon in the absence of a magnetic field, are then "isospin-up," which we arbitrarily assign to the proton, and "isospin-down," the neutron.† That is, for a nucleon with isospin quantum number $t = \frac{1}{2}$, a proton has $m_t = +\frac{1}{2}$ and a neutron has $m_t = -\frac{1}{2}$. These projections are measured with respect to an arbitrary axis called the "3-axis" in a coordinate system whose axes are labeled 1, 2, and 3, in order to distinguish it from the laboratory z axis of the x, y, z coordinate system. The isospin obeys the usual rules for angular momentum vectors; thus we use an isospin vector $\boldsymbol{t}$ of length $\sqrt{t(t+1)}\,\hbar$ and with 3-axis projections $t_3 = m_t\hbar$.

For a system of several nucleons, the isospin follows coupling rules identical with the rules of ordinary angular momentum vectors. A two-nucleon system, for example, can have total isospin T of 0 or 1, corresponding (semiclassically) to the antiparallel or parallel orientations of the two isospin-$\frac{1}{2}$ vectors. The 3-axis component of the total isospin vector, T_3, is the sum of the 3-axis components of the individual nucleons, and thus for any nucleus,

$$T_3 = \tfrac{1}{2}(Z - N) \tag{11.12}$$

expressed in units of $\hbar$ which will not be shown explicitly.

For a given nucleus, T_3 is determined by the number of neutrons and protons. For any value of T_3, the total isospin quantum number T can take any value at least as great as $|T_3|$. Two related questions that immediately follow are: Can we assign the quantum number T to individual nuclear states? Is such an assignment useful, for example, in predicting decay or reaction probabilities?

We consider as an example the two-nucleon system, which can have T of 0 or 1. There are thus four possible 3-axis components: $T_3 = +1$ (two protons), $T_3 = -1$ (two neutrons), and two combinations with $T_3 = 0$ (one proton and one neutron). The first two states must have $T = 1$, while the latter two can have $T = 0$ and $T = 1$. If the nuclear interaction is perfectly charge independent (and if we "turn off" the electromagnetic interaction), then the three 3-axis projections of $T = 1$ $(+1, 0, -1)$ must have the same energy, while the single $T = 0$ state may have a different energy. In fact, we know that the isospin triplet (which is the $I = 0$ singlet of ordinary spin) is unbound, as discussed in Chapter 4.

*Isospin is often called *isotopic spin* or *isobaric spin*, the former because the value of its projection, equal to $\frac{1}{2}(Z - N)$, distinguishes between isotopes and the latter because the isospin quantum number is valid to label isobaric multiplets. The name "isospin" avoids the controversy and is now the generally accepted term.

†Originally, nuclear physicists defined the neutron as the isospin-up member of the nucleon family. Particle physicists also use isospin to label the different charge states of strongly interacting particles, but they stress the connection with electric charge by choosing isospin-up for the proton. This choice has now been accepted by nuclear physicists as well.

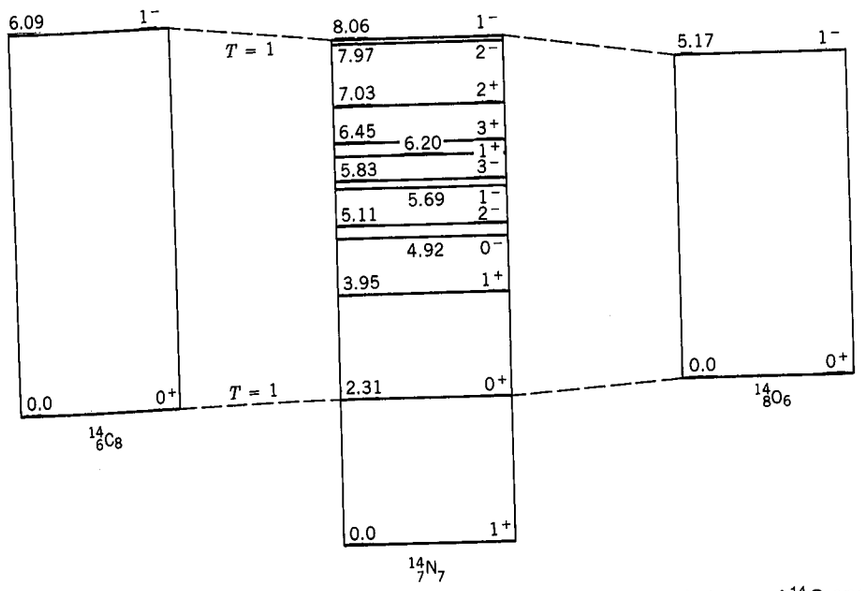

Figure 11.5 Lower energy levels of $A = 14$ isobars. The ground states of ^{14}C and ^{14}O have been shifted relative to ^{14}N by the neutron-proton mass difference and the Coulomb energy; the respective shifts are 2.36 and 2.44 MeV. Energy levels in ^{14}C and ^{14}O have $T = 1$; levels in ^{14}N have $T = 0$ except the $T = 1$ levels at 2.31 and 8.06 MeV. Based on data compiled by F. Ajzenberg-Selove, *Nucl. Phys. A* **449**, 53 (1986).

A clearer example of the isospin assignments can be found in the nuclei of the $A = 14$ system. Figure 11.5 shows the states of ^{14}C ($T_3 = -1$), ^{14}N ($T_3 = 0$), and ^{14}O ($T_3 = +1$). For ^{14}N, we know that any integer T can give a 3-axis component of 0, and the possible values of T therefore range from 0 up to a maximum of $A/2$ or 7. The tendency toward nuclear symmetry (reflected in the symmetry term of the semiempirical mass formula) implies that the lowest states will most likely have $T = |T_3|$, that is, the smallest possible value of T. This will certainly apply to the ground state, but the excited states must be assigned on the basis of reaction or decay studies or symmetry arguments. In Figure 11.5, the energies have been adjusted so that the neutron-proton mass difference (an electromagnetic effect) and the Coulomb energy of the nucleus have been removed. The energies of the states should then be due only to the nuclear force. Note that the energies of the 0^+ states in the three nuclei are nearly identical; these are the states of the $T = 1$ triplet. Similar agreement is obtained for the 1^- triplet.

Such speculations regarding the T assignments can be verified through decay and reaction studies. For example, angular momentum coupling theory leads to selection rules for $E1$ transitions: ΔT must be 0 or ± 1, except that transitions from $T = 0$ to $T = 0$ are forbidden and $\Delta T = 0$ transitions are forbidden in nuclei with $T_3 = 0$. To test these rules, we examine the half-lives for the 1^- to 0^+ $E1$ transitions in ^{14}O, ^{14}C, and ^{14}N. The measured half-lives of the analogous states are, respectively, 1.2×10^{-4}, < 7, and 27 fs. The ^{14}N transition, which is a

$\Delta T = 0$ $E1$ transition in a $T_3 = 0$ nucleus, is forbidden by the isospin selection rule and is indeed strongly inhibited, as its longer half-life indicates. (The Weisskopf estimate for the half-life is about 7×10^{-3} fs.)

Consider also the decay of the 1^-, $T = 0$ level at 5.69 MeV in ^{14}N. The $E1$ decay to the 1^+, $T = 0$ ground state should be inhibited by the selection rule, while the $E1$ decay to the 0^+, $T = 1$ level at 2.31 MeV is permitted. The higher energy transition ought to be greater in intensity by about a factor of 5, owing to the E^3 dependence of the $E1$ transition probability, yet the lower energy transition is observed to have about twice the intensity. The effect of the isospin selection rule is a reduction in the expected relative intensity of the 5.69-MeV $E1$ transition by about an order of magnitude.

Similar selection rules operate in β decay. The Fermi matrix element is forbidden unless $\Delta T = 0$, which is the case in the mirror decays listed in the top half of Table 9.3. The nonmirror decays are those with $\Delta T = 1$, and the Fermi contribution to the transition is reduced by several orders of magnitude by the violation of the isospin selection rule. The 0^+ to 0^+ decays, which on the basis of ordinary angular momentum alone should be pure Fermi decays of the superallowed category as in Table 9.2, are inhibited by three orders of magnitude if $\Delta T \neq 0$; the log ft values rise from about 3.5 for the $\Delta T = 0$ decays permitted by the isospin selection rule to 7 or larger for the $\Delta T \neq 0$ isospin-forbidden decays.

Nuclear reactions also show effects of isospin. Because the nuclear force does not distinguish between protons and neutrons, the isospin must be absolutely conserved in all nuclear reactions. The 3-axis component is automatically conserved when the numbers of protons and neutrons remain constant, but it is also true that the total isospin quantum number T remains invariant in reactions. Consider the reaction $^{16}\text{O} + {}^2\text{H} \rightarrow {}^{14}\text{N} + {}^4\text{He}$, leading to states in ^{14}N. All four reacting particles have $T = 0$ ground states; thus T is conserved if the product particles remain in their ground states. Excitation of ^{4}He is unlikely in low-energy reactions, for its first excited state is above 20 MeV, and thus it is expected that only $T = 0$ excited states in ^{14}N can be reached in the reaction; the 2.31-MeV, $T = 1$ state should not be populated. Any small population observed for that state must arise from isospin impurities in the reacting particles. The cross section to reach the 2.31-MeV state is observed to be about 2 orders of magnitude smaller than the cross sections to reach the neighboring $T = 0$ states, showing the effectiveness of the isospin selection rule. In the similar reaction $^{12}\text{C}(\alpha, \text{d})^{14}\text{N}$ the cross section for the 2.31-MeV state is 3 orders of magnitude smaller than the isospin-allowed cross sections, and in $^{10}\text{B}(^6\text{Li}, \text{d})^{14}\text{N}$ and $^{12}\text{C}(^6\text{Li}, \alpha)^{14}\text{N}$ it is at least two orders of magnitude smaller. By way of contrast, in $^{10}\text{B}(^7\text{Li}, ^3\text{H})^{14}\text{N}$, the $T = 1$ level is populated with a strength comparable to that of the neighboring $T = 0$ level; the isospin selection rule does not inhibit the probability to reach the $T = 1$ level. (The initial nuclei have a total T of $\frac{1}{2}$; the $\frac{1}{2}$ isospin of ^{3}H can couple to either $T = 0$ or $T = 1$ in ^{14}N to give a resultant of $\frac{1}{2}$.)

The members of an isospin multiplet, as for example pairs of mirror nuclei or a set of the three states connected by the dashed lines in Figure 11.5, are called *isobaric analog states*, a term which was previously introduced in the discussion of β decay in Section 9.8. The analog states in neighboring nuclei have identical nucleon wave functions, except for the change in the number of protons and neutrons. In the ^{14}C and ^{14}O ground states, the nucleons are strongly coupled

pairwise (with two coupled proton holes in ^{14}C and two coupled neutron holes in ^{14}O), and the 2.31-MeV analog state in ^{14}N must have a similar wave function, with the odd proton hole and neutron hole strongly paired.

Because analog states are obtained by exchanging a proton for a neutron, they tend to be strongly populated in β decay (see Figure 9.17) and in (p, n) or (n, p) reactions. In medium and heavy nuclei, placing a proton into a state formerly occupied by a neutron involves a large energy transfer, because with $N > Z$ the newly placed neutron occupies a considerably higher shell-model state than the former proton. Analog states may appear in medium and heavy nuclei at energies of 10 MeV and above, and thus they generally do not contribute to low-energy reaction and decay studies.

11.4 REACTION CROSS SECTIONS

In Chapter 4 we considered the nature of cross sections and the application to nucleon-nucleon scattering. In this section we give some more general definitions of various measurable quantities that are loosely grouped under the heading "cross section."

Roughly speaking, the cross section is a measure of the relative probability for the reaction to occur. If we have a detector placed to record particle b emitted in a direction (θ, ϕ) with respect to the beam direction, the detector defines a small solid angle $d\Omega$ at the target nucleus (Figure 11.6). Let the current of incident particles be I_a particles per unit time, and let the target show to the beam N target nuclei per unit area. If the outgoing particles appear at a rate R_b, then the reaction cross section is

$$\sigma = \frac{R_b}{I_a N} \tag{11.13}$$

Defined in this way, σ has the dimension of area per nucleus, but it may be very much larger or smaller than the geometrical area of the disc of the target nucleus

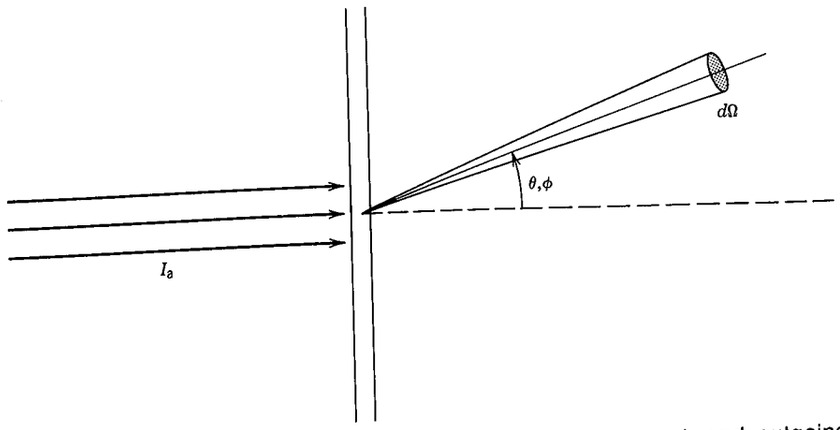

Figure 11.6 Reaction geometry showing incident beam, target, and outgoing beam going into solid angle $d\Omega$ at θ, ϕ.

seen by the incoming beam. For a typical nucleus of radius $R = 6$ fm, the geometrical area πR^2 is about 100 fm^2 = 1 b; for neutron capture by ^{135}Xe, the cross section is about 10^6 b, while for other much more improbable reactions the cross section may be measured in millibarns or microbarns. You should think of σ as a quantity which has the dimension of an area, but which is proportional to the reaction probability.

Our detector occupies only a small solid angle $d\Omega$ and therefore does not observe *all* of the outgoing particles; only a small fraction dR_b are actually counted, and therefore only a fraction of the cross section $d\sigma$ will be deduced. Moreover, the outgoing particles will not in general be emitted uniformly in all directions, but will have an angular distribution that will depend on θ and possibly also on ϕ. It we let this angular distribution function be arbitrarily represented by $r(\theta, \phi)$, then $dR_b = r(\theta, \phi)\, d\Omega/4\pi$. (The 4π is introduced to make $d\Omega/4\pi$ a pure fraction.) Then

$$\frac{d\sigma}{d\Omega} = \frac{r(\theta, \phi)}{4\pi I_a N} \tag{11.14}$$

The quantity $d\sigma/d\Omega$ is called the *differential cross section*, and its measurement gives us important information on the angular distribution of the reaction products. In the literature, it is often called $\sigma(\theta, \phi)$ or $\sigma(\theta)$ or sometimes (unfortunately) just "cross section." (If you see a graph of "cross section" vs θ, you should know that what is intended is differential cross section.) Because solid angle is measured in steradians (the surface of a sphere subtends a solid angle of 4π steradians at its center), units of differential cross section are barns/steradian. The reaction cross section σ can be found by integrating $d\sigma/d\Omega$ over all angles; with $d\Omega = \sin\theta\, d\theta\, d\phi$ we have*

$$\sigma = \int \frac{d\sigma}{d\Omega}\, d\Omega = \int_0^{\pi} \sin\theta\, d\theta \int_0^{2\pi} d\phi\, \frac{d\sigma}{d\Omega} \tag{11.15}$$

Notice that if $d\sigma/d\Omega$ is constant (independent of angle), the integral gives $\sigma = 4\pi(d\sigma/d\Omega)$. This justifies the insertion of the constant 4π into Equation 11.14, for now $r(\theta, \phi)$ reduces to the constant R_b and Equation 11.14 agrees with Equation 11.13.

In many nuclear physics applications, we are not concerned simply with the probability to find particle b emitted at a certain angle; we also want to find it with a certain energy, corresponding to a particular energy of the residual nucleus Y. We therefore must modify the definition of cross section to give the probability to observe b in the angular range of $d\Omega$ and in the energy range dE_b. This gives the so-called *doubly differential cross section* $d^2\sigma/dE_b\, d\Omega$. In the literature, this additional energy dependence is often not explicitly stated; usually the cross sections are plotted as $d\sigma/d\Omega$ vs θ *leading to a specific final energy state*. This is in reality $d^2\sigma/dE_b\, d\Omega$, although it may not be labeled as such. For discrete states, there may be only a single level within the energy range dE_b, and the

*An element of area on the surface of a sphere is $r^2\, d\Omega$ or $r^2 \sin\theta\, d\theta\, d\phi$ in spherical coordinates. Hence $d\Omega = \sin\theta\, d\theta\, d\phi$.

Table 11.1 Reaction Cross Sections

Cross Sections	Symbol	Technique	Possible Application
Total	σ_t	Attenuation of beam	Shielding
Reaction	σ	Integrate over all angles and all energies of b (all excited states of Y)	Production of radioisotope Y in a nuclear reaction
Differential (Angular)	$d\sigma/d\Omega$	Observe b at (θ, ϕ) but integrate over all energies	Formation of beam of b particles in a certain direction (or recoil of Y in a certain direction)
Differential (Energy)	$d\sigma/dE$	Don't observe b, but observe excitation of Y by subsequent γ emission	Study of decay of excited states of Y
Doubly differential	$d^2\sigma/dE_b\, d\Omega$	Observe b at (θ, ϕ) at a specific energy	Information on excited states of Y by angular distribution of b

distinction becomes unimportant. If, on the other hand, we do not observe the direction of particle b (by surrounding the target area with 4π solid angle of detectors, or by not observing b at all), then we measure yet another differential cross section $d\sigma/dE$, where now E may represent an excitation energy of Y.

There is still another cross section that may be of interest, the *total cross section* σ_t. Here, for a specific incident particle a, we add the reaction cross sections σ for all possible different outgoing particles b, no matter what their direction or energy. Such a determination would tell us the probability for an incident particle to have *any reaction at all* with the target and thus be removed from the beam of incident particles. This can be deduced directly by measuring the loss in intensity of a collimated beam in passing through a certain thickness of the target material.

When we discuss a specific reaction then, the exact meaning of the term cross section will depend on exactly what we measure. Table 11.1 summarizes these different measurements, how they might be accomplished, and the application to which the result might be put. For example, if we wish to produce a radioactive isotope as the residual nucleus Y, we have absolutely no interest in the direction of emission of particle b, nor in the excited states of Y that may be populated, for they will quickly decay by γ emission to the ground state of Y. The literature often does not discriminate carefully among these definitions, and often they are called merely "cross section." It is almost always obvious in context which cross section is meant, and therefore not strictly necessary to distinguish carefully among them.

11.5 EXPERIMENTAL TECHNIQUES

A typical nuclear reaction study requires a beam of particles, a target, and a detection system. Beams of charged particles are produced by a variety of different types of accelerators (see Chapter 15), and neutron beams are available from nuclear reactors and as secondary beams from charged-particle accelerators. To do precision spectroscopy of the outgoing particle b and the residual nucleus Y, the beam must satisfy several criteria:

1. It must be *highly collimated and focused*, so that we have a precise reference direction to determine θ and ϕ for angular distribution measurements.
2. It must have a *sharply defined energy*; otherwise, in trying to observe a specific excited state by finding Q_{ex} and E_{ex} from Equation 11.5, we might find that variations in T_a would give two or more different E_{ex} for the same T_b.
3. It must be of *high intensity*, so that we can gather the necessary statistics for precise experiments.
4. If we wish to do timing measurements (such as to measure the lifetimes of excited states of Y), the beam must be *sharply pulsed* to provide a reference signal for the formation of the state, and the pulses must be separated in time by at least the time resolution of the measuring apparatus and preferably by a time of the order of the one we are trying to measure.
5. Under ideal circumstances, the accelerator beam should be *easily selectable*—we should be able to change the incident energy T_a or even the type of incident particle in a reasonable time. The stringent tuning requirements of modern large accelerators and the demands that high currents put on ion sources make this requirement hard to meet in practice. Accelerator beam time is often scheduled far in advance (6 months to a year is common), so that experiments with common beam requirements can be grouped together, thus minimizing the beam tuning time.
6. The intensity of the incident beam should be nearly *constant and easily measurable*, for we must know it to determine the cross section. If we move a detector from one position to another, we must know if the change in the observed rate of detection of particle b comes from the angular dependence of the differential cross section or merely from a change in the incident beam intensity.
7. The beam may be *polarized* (that is, the spins of the incident particles all aligned in a certain direction) or *unpolarized*, according to the desire of the experimenters.
8. The beam must be transported to the target through a *high-vacuum system* so as to prevent beam degradation and production of unwanted products by collisions with air molecules.

Types of targets vary widely, according to the goals of the experiment. If we want to measure the yield of a reaction (that is, σ or σ_t), perhaps through observation of the attenuation of the beam or the decay of radioisotope Y, then we may choose a thick, solid target. Such a target might degrade, scatter, or even

stop the outgoing particles b, which does not bother us in this kind of measurement. On the other hand, if we wish to observe b unaffected by interactions in the target, a very thin target is required. Thin metal foils are often used as targets, but for nonmetals, including compounds such as oxides, the target material is often placed on a thin backing, which does not contribute to the reaction or affect the passage of particle b. For many applications, extremely rare (and often expensive) targets of separated isotopes are used. A high-intensity, highly focused beam (typically a few mm in diameter) delivers considerable thermal power to the target (absorption of 1 μA of 10 MeV protons delivers 10 W), which is enough to burn up thin targets; therefore a way must be found to cool the target and extract the heat generated by the beam. As with the beam, it should be relatively easy to change targets so that valuable beam time is not wasted. For some applications, it may be desirable to polarize the spins of the target nuclei.

The detectors may consist of some (or all) of the following: particle detectors or detector telescopes to determine the energy and type of the outgoing particles, magnetic spectrometers for good energy resolution (sometimes necessary to identify close-lying excited states of Y), position-sensitive particle detectors (such as multiwire proportional counters) to do accurate angular distribution work, γ-ray detectors to observe the de-excitation of the excited states of Y (possibly in coincidence with particle b), polarimeters to measure the polarization of the particles b, and so on. Because beam time is a precious commodity at a modern accelerator facility, the emphasis is always on getting the largest amount of data in the shortest possible time. Therefore multidetector configurations are very common; many signals arrive simultaneously at the detectors and are stored by an on-line computer system for later "re-play" and analysis. (Keeping the beam and the detectors going during the experiment usually demands all the attention of the experimenters and leaves little time for data analysis!)

11.6 COULOMB SCATTERING

Because the nucleus has a distribution of electric charge, it can be studied by the electric (Coulomb) scattering of a beam of charged particles. This scattering may be either elastic or inelastic.

Elastic Coulomb scattering is called *Rutherford scattering* because early (1911–1913) experiments on the scattering of α particles in Rutherford's laboratory by Geiger and Marsden led originally to the discovery of the existence of the nucleus. The basic geometry for the scattering is shown in Figure 11.7. As is always the case for unbound orbits in a $1/r^2$ force, the scattered particle follows a hyperbolic path. (We will assume the target nucleus to be infinitely massive, so that the scattering center remains fixed.) The particle approaches the target nucleus along a straight line that would pass a distance b from the nucleus in the absence of the repulsive force; this distance is called the *impact parameter*. The scattering angle is θ. Very far from the nucleus, the incident particle has negligible Coulomb potential energy; its total energy is thus only the incident kinetic energy $T_a = \frac{1}{2}mv_0^2$. Its angular momentum relative to the target nucleus is $|\boldsymbol{r} \times m\boldsymbol{v}| = mv_0 b$ at large distances. In passing close to the target nucleus, the particle reaches a minimum separation distance r_{min} (which depends on b), the

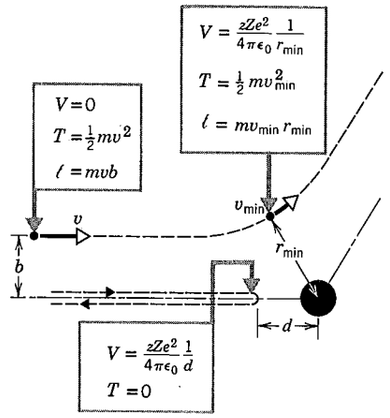

Figure 11.7 The trajectory of a particle undergoing Rutherford scattering, showing the closest approach to the target nucleus.

absolute minimum value of which occurs in a head-on collision ($b = 0$), in which the particle comes instantaneously to rest before reversing its motion. At this point it has exchanged its initial kinetic energy for Coulomb potential energy:

$$\tfrac{1}{2}mv_0^2 = \frac{1}{4\pi\epsilon_0}\frac{zZe^2}{d} \tag{11.16}$$

where ze is the charge of the projectile and Ze the target. The distance d is called the *distance of closest approach*. At intermediate points in the trajectory, the energy is partly kinetic and partly potential; conservation of energy gives (for any value of the impact parameter)

$$\tfrac{1}{2}mv_0^2 = \tfrac{1}{2}mv^2 + \frac{1}{4\pi\epsilon_0}\frac{zZe^2}{r} \tag{11.17}$$

The scattering has cylindrical symmetry about the beam axis (because the Coulomb force is symmetric), and therefore the cross section is independent of the azimuthal angle ϕ. We therefore work in a ring or annular geometry (Figure 11.8). Particles with impact parameters between b and $b + db$ are scattered into the ring at angles between θ and $\theta + d\theta$. Let the target have n nuclei per unit volume, and assume the target to be thin enough so that it is unlikely to have any "shadowing" of one nucleus by another. The target is considered to be a foil of thickness x. Then the number of nuclei per unit area is nx, and the fraction df of the incident particles that pass through the annular ring of area $2\pi b\,db$ is

$$df = nx(2\pi b\,db) \tag{11.18}$$

The fraction f with impact parameters less than b is

$$f = nx\pi b^2 \tag{11.19}$$

If particles scattered with impact parameter b emerge at angle θ, then Equation 11.19 also gives the fraction that are scattered at angles greater than θ, but to carry the discussion further we need a relationship between b and θ. (We are

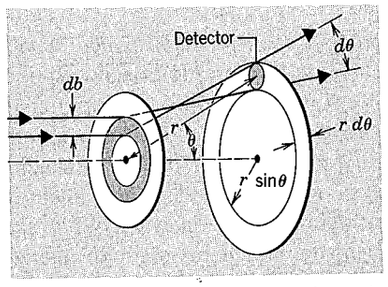

Figure 11.8 Particles entering the ring between b and $b + db$ are distributed uniformly along a ring of angular width $d\theta$. A detector is at a distance r from the scattering foil.

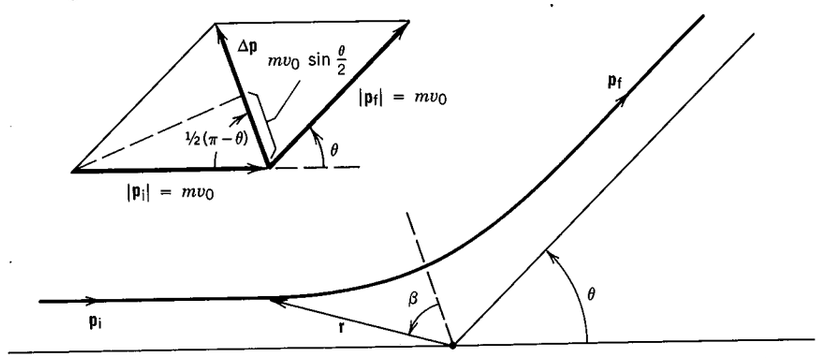

Figure 11.9 The hyperbolic trajectory of a scattered particle. The instantaneous coordinates are r, β. The change in momentum is $\Delta \boldsymbol{p}$, in the direction of the dashed line that bisects $(\pi - \theta)$.

assuming that each incident particle is scattered only once—more about this assumption later.)

The net linear momentum of the scattered particles changes in direction only; far from the scattering, the incident and the final linear momentum are both mv_0. (This follows from the assumption that the target is so massive that it does not move.) The change in the momentum vector, as shown in Figure 11.9, is a vector of magnitude

$$\Delta p = 2mv_0 \sin \frac{\theta}{2} \tag{11.20}$$

in the direction of the bisector of $\pi - \theta$. According to Newton's second law in the form $F = dp/dt$, this is equal to the net impulse of the Coulomb force in that direction:

$$\Delta p = \int dp = \int F\,dt = \frac{zZe^2}{4\pi\epsilon_0} \int \frac{dt}{r^2} \cos\beta \tag{11.21}$$

where β is the angle between the bisector and instantaneous vector $\boldsymbol{r}$ locating the particle. In the initial position far from the scattering, which we take to be time $t = 0$, the angle β has the value $-(\pi/2 - \theta/2)$; in the final position ($t = \infty$), the angle β is $+(\pi/2 - \theta/2)$.

The instantaneous velocity $\boldsymbol{v}$ can be written in terms of radial (along $\boldsymbol{r}$) and tangential components:

$$\boldsymbol{v} = \frac{dr}{dt}\hat{r} + r\frac{d\beta}{dt}\hat{\beta} \tag{11.22}$$

where $\hat{r}$ and $\hat{\beta}$ indicate unit vectors in the radial and tangential directions, respectively. Only the tangential component contributes to the angular momentum about the nucleus:

$$\ell = |m\boldsymbol{r} \times \boldsymbol{v}| = mr^2\frac{d\beta}{dt} \tag{11.23}$$

Far from the nucleus, the angular momentum has the value mv_0b; conservation of angular momentum gives

$$mv_0b = mr^2\frac{d\beta}{dt}$$

$$\frac{dt}{r^2} = \frac{d\beta}{v_0b} \tag{11.24}$$

and substituting into Equation 11.21 gives

$$\Delta p = \frac{zZe^2}{4\pi\epsilon_0 v_0 b}\int_{-(\pi/2-\theta/2)}^{+(\pi/2-\theta/2)} \cos\beta\,d\beta$$

$$= \frac{zZe^2}{2\pi\epsilon_0 v_0 b}\cos\frac{\theta}{2} \tag{11.25}$$

Combining this result with Equation 11.20 gives the needed relationship between b and θ:

$$b = \frac{d}{2}\cot\frac{\theta}{2} \tag{11.26}$$

where d is the distance of closest approach from Equation 11.16. Combining Equations 11.18 and 11.26,

$$|df| = \pi n x \frac{d^2}{4}\cot\frac{\theta}{2}\csc^2\frac{\theta}{2}\,d\theta \tag{11.27}$$

and the rate at which particles reach the ring, per unit solid angle, is

$$r(\theta, \phi) = \frac{I_a|df|}{d\Omega/4\pi} \tag{11.28}$$

where I_a is the rate at which incident particles fall on the target (and hence $I_a|df|$ is the number that fall between b and $b + db$). With $d\Omega = 2\pi \sin\theta\,d\theta$ for the ring geometry (that is, $\sin\theta\,d\theta\,d\phi$ integrated over ϕ), the net result is

$$\frac{d\sigma}{d\Omega} = \left(\frac{zZe^2}{4\pi\epsilon_0}\right)^2\left(\frac{1}{4T_a}\right)^2\frac{1}{\sin^4\dfrac{\theta}{2}} \tag{11.29}$$

This is the differential cross section for Rutherford scattering, usually called the

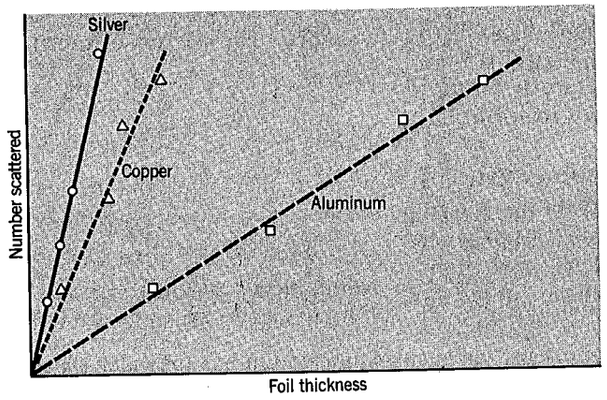

(a)

Figure 11.10 (*a*) The dependence of scattering rate on foil thickness for three different scattering foils.

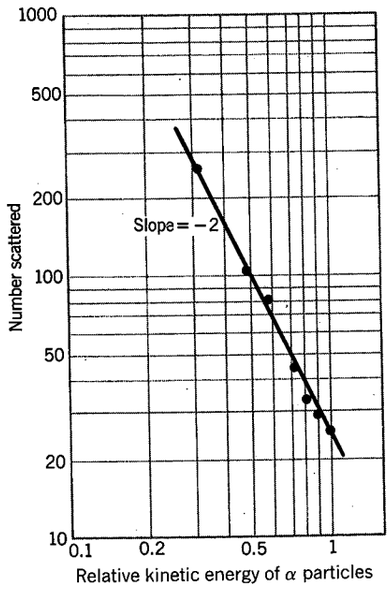

(c)

Figure 11.10 (*c*) The dependence of scattering rate on the kinetic energy of the incident α particles for scattering by a single foil. Note the log-log scale; the slope of -2 shows that $\log N \propto -2 \log T$, or $N \propto T^{-2}$, as expected from the Rutherford formula.

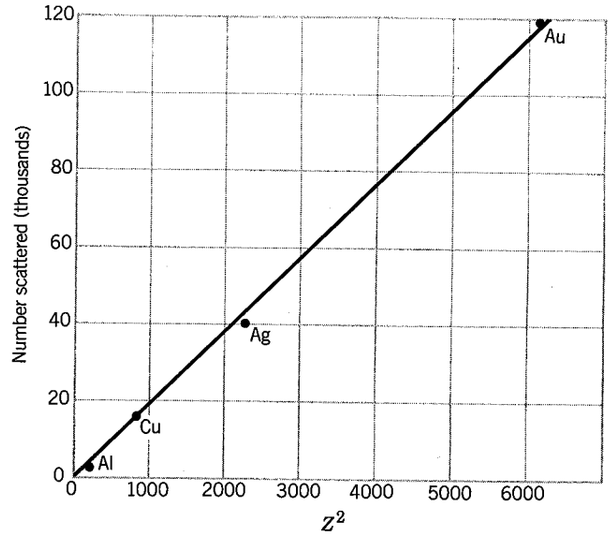

(b)

Figure 11.10 (*b*) The dependence of scattering rate on the nuclear charge Z for foils of different materials. The data are plotted against Z^2

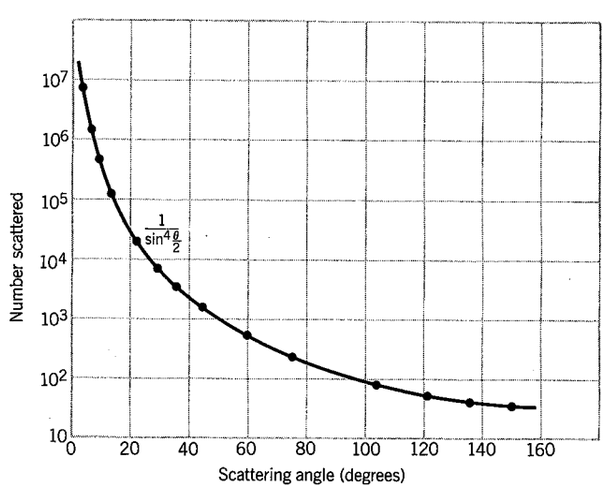

(d)

Figure 11.10 (*d*) The dependence of scattering rate on the scattering angle θ, using a gold foil. The $\sin^{-4}(\theta/2)$ dependence is exactly as predicted by the Rutherford formula.

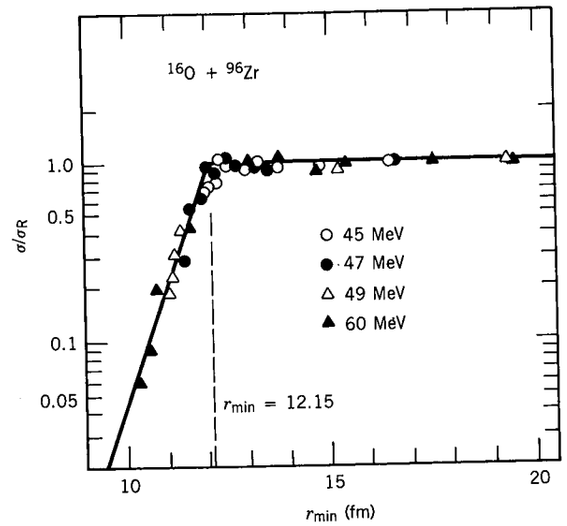

Figure 11.11 Elastic scattering of ^{16}O from ^{96}Zr at several incident energies. The horizontal axis shows the minimum separation distance r_{min} between projectile and target, which varies with b and therefore with θ. The vertical axis shows the cross section in terms of the calculated Rutherford cross section. Nuclear scattering effects appear at separations of less than 12.15 fm; this corresponds to $R_0 = 1.7$ fm, considerably greater than the mean radius of 1.25 fm, but consistent with a "skin thickness" of about 0.5 fm which allows the two nuclear distributions to overlap at these larger distances. From P. R. Christensen et al., *Nucl. Phys. A* **207**, 33 (1973).

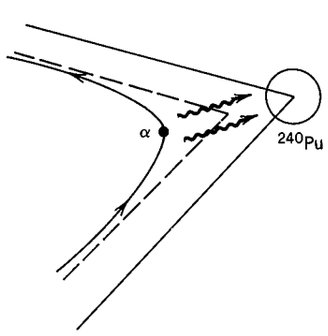

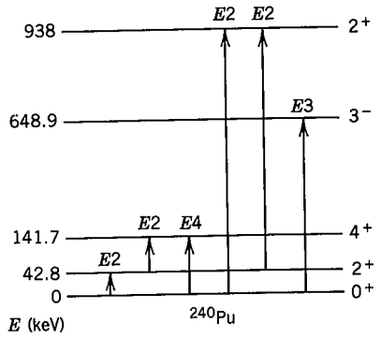

Figure 11.12 Inelastic Coulomb scattering (Coulomb excitation). The projectile exchanges energy with the target through the Coulomb interaction (exchanged photons are shown as wavy lines) and the target ^{240}Pu, originally in its ground state, can be driven to excited states. Several different modes of excitation are shown, including two-step processes. The spectrum of inelastically scattered α's shows which excited states of ^{240}Pu have been excited. Data from C. E. Bemis, Jr., et al., *Phys. Rev. C* **8**, 1466 (1973).

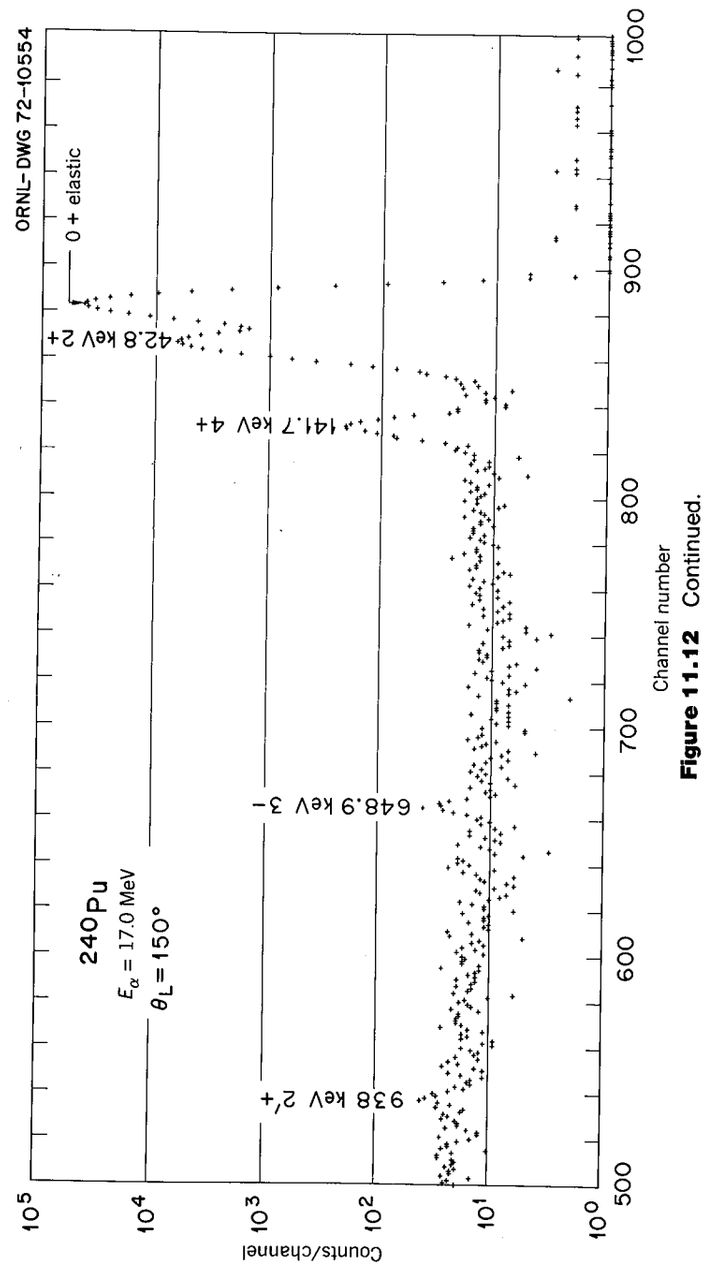

Figure 11.12 Continued.

Rutherford cross section. Note especially the $\sin^{-4}(\theta/2)$ dependence, which is characteristic.

In a difficult and painstaking series of experiments, Geiger and Marsden verified three aspects of the Rutherford formula: the dependence on Z^2, T_a^{-2}, and $\sin^{-4}(\theta/2)$. Figure 11.10 shows the excellent agreement with the predictions of the formula.

The most noteworthy aspect of the scattering experiment, and the detail that led Rutherford to his concept of the nuclear atom, is the fraction scattered at large angles, say beyond 90°. For example, we consider a gold foil of thickness 2.0×10^{-4} cm, on which 8.0 MeV α's are incident. From Equation 11.26, we find $b = 14$ fm, from which Equation 11.19 gives $f = 7.5 \times 10^{-5}$. This is a large fraction to be scattered at such angles and requires a dense, compact nucleus as the scatterer.

Let's look at the situation for small angles. For the above gold foil, there are about 12×10^{18} nuclei/cm^2, or of the order of 0.003 nm lateral spacing between nuclei, as seen by an incoming α particle. This means about $\frac{2}{3}$ of the α particles have an impact parameter of 0.001 nm or greater. For this impact parameter, the scattering angle is 1.6°. Thus the mean scattering angle is of order 1° or less. To appear at large angles, we must have either many scatterings, each at a small angle, or a single scattering at large angle. Of course, if there are many individual scatterings of a random nature, some will tend to increase the net scattering angle and others will tend to decrease it. To observe scattering at a total angle of about $N\theta_{\text{mean}}$, there must be about N^2 individual scatterings. If we observe scattering at a fixed angle θ much larger than 1° and if we vary the thickness x of the scattering foil, then we expect the probability to observe scattered particles to vary as $\sqrt{x}$ for multiple scattering, while it should vary with x in the case of single scattering (simply because there are linearly more chances to have single large-angle scattering as the number of nuclei increases). Figure 11.10*a* shows the variation of the number of scattered particles with x, and the linear behavior is quite apparent.

Our treatment of Rutherford scattering has been based entirely on classical concepts; no quantum effects are included. In particular, the uncertainty principle renders doubtful any treatment based on fixed trajectories and particle orbits. Any attempt to locate a particle with an impact parameter of arbitrarily small uncertainty would introduce a large uncertainty in the transverse momentum and thus in the scattering angle. We are not discussing the experimental difficulty of "aiming" a beam with a specific impact parameter; the range of impact parameters is automatically included in the variation with θ of $d\sigma/d\Omega$. What we discuss here is whether the assumption of a definite trajectory has introduced pathological errors into the derivation of the Rutherford cross section.

Corresponding to an uncertainty Δb in the impact parameter will be an uncertainty Δp in the transverse momentum of order $\hbar/\Delta b$. Our classical derivation makes sense only if $\Delta b \ll b$ and $\Delta p \ll p_{\text{transverse}}$:

$$b\,\Delta p_{\text{transverse}} \gg \Delta b\,\Delta p \gtrsim \hbar$$

$$\frac{b\,\Delta p_{\text{transverse}}}{\hbar} \gg 1 \qquad (11.30)$$

We consider two extreme cases: (1) 90° scattering, for which $b = d/2 = 14$ fm and $\Delta p_{\text{transverse}} = mv_0 = 250$ MeV/c, where we have assumed 8-MeV α's incident on gold. For this case the ratio in Equation 11.30 is about 18, reasonably far from the quantum limit. (2) Small-angle scattering ($\theta \simeq 1°$), with $b = 1600$ fm and $\Delta p_{\text{transverse}} \simeq mv_0 \tan\theta \simeq 4$ MeV/c. The ratio is now about 32, again far from the quantum limit.

Ultimately what justifies the classical calculation is a happy accident of quantum physics: the quantum calculation of the Coulomb scattering cross section gives the same result as the classical calculation, Equation 11.29. This is a peculiarity of the $1/r^2$ force, in which the exact quantum result contains no factors of $\hbar$, and thus the "classical limit" of $\hbar \to 0$ leaves the quantum result unchanged.

As we increase the energy of the incident particle, we will eventually reach a point where the distance of closest approach decreases to the nuclear radius, and thus the projectile and target feel each other's nuclear force. The Rutherford formula, which was derived on the basis of Coulomb interactions only, fails at that point to account for the cross section, as we illustrated in Figure 3.11. (The cross section then includes Coulomb and nuclear parts, as in the case of proton-proton scattering, Equation 4.43.) The internuclear separation at which the Rutherford formula fails is then a measure of the nuclear radius, as illustrated in Figure 11.11.

Up to now we have considered only elastic Coulomb scattering. Inelastic Coulomb scattering is called *Coulomb excitation*; after the encounter the nucleus (and possibly, although not usually, the projectile) is left in an excited state, from which it decays rapidly with the emission of γ rays. We can think of this process as the emission and absorption of virtual photons, with the most likely mode being $E2$. This process has therefore been extensively used to study the first excited 2^+ states of even-Z, even-N nuclei. Because the $0^+ \to 2^+$ photon absorption probability is closely related to the $2^+ \to 0^+$ photon emission probability, the Coulomb excitation probability can give a measure of the half-life of the 2^+ state. Moreover, since the 2^+ state lives much longer than the time it takes for the encounter between target and projectile, there is a second-order interaction between the projectile and the excited-state nuclei of the target. This can have several effects, including photon absorption causing a $2^+ \to 4^+$ upward transition and a change in the m-state population of the 2^+ state from the interaction of its quadrupole moment with the electric field gradient of the moving projectile.

Figure 11.12 shows some sample results from inelastic Coulomb scattering. The reduced energy of the detected particles exactly matches the energy simultaneously observed in γ-ray emission from the excited states.

11.7 NUCLEAR SCATTERING

The elastic nuclear scattering of particles bears a strong resemblance to a familiar problem from optics: the diffraction of light by an opaque disk (Figures 4.3 and 11.13). In the optical case, diffraction at the sharp edge results in a series of maxima and minima; the first minimum occurs at $\theta \sim \lambda/R$, the succeeding minima are roughly (but not exactly) equally spaced, and the intervening maxima are of steadily and substantially decreasing intensity.

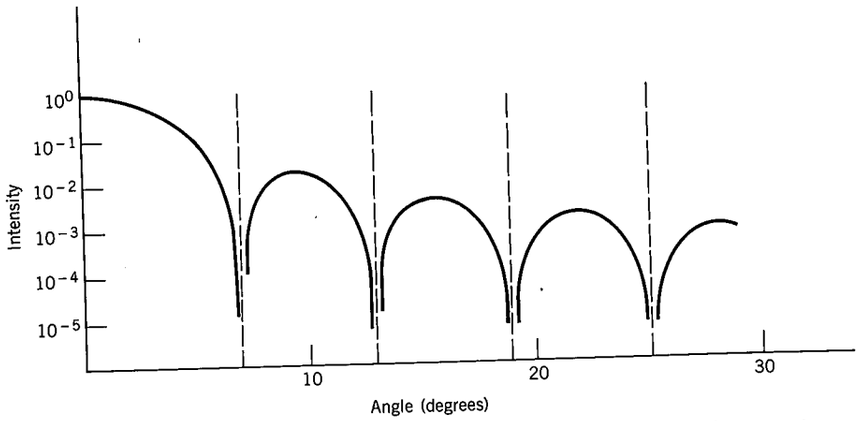

Figure 11.13 Diffraction pattern of light incident on a circular aperture; a circular disk gives a similar pattern. The minima have intensity of zero. The curve is drawn for a wavelength equal to ten times the diameter of the aperture or disk.

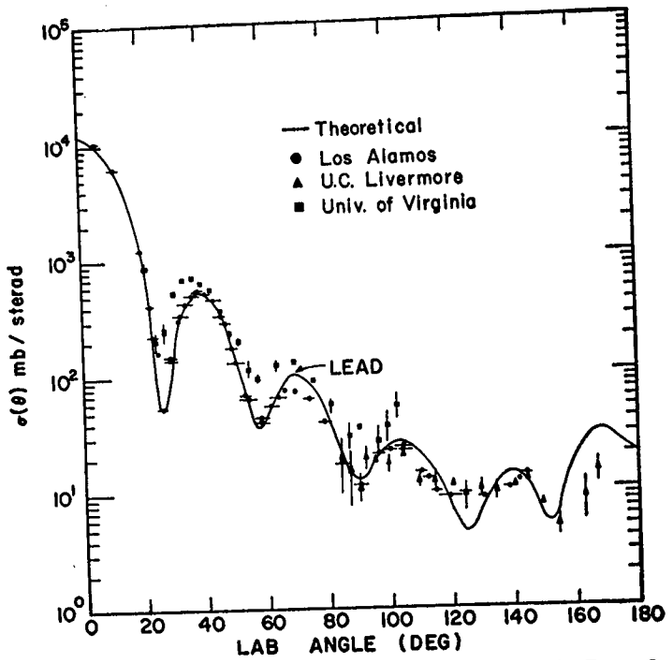

Figure 11.14 Elastic scattering of 14-MeV neutrons from Pb. From S. Fernbach, *Rev. Mod. Phys.* **30**, 414 (1958).

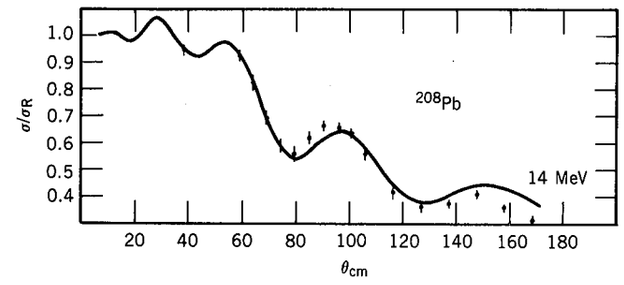

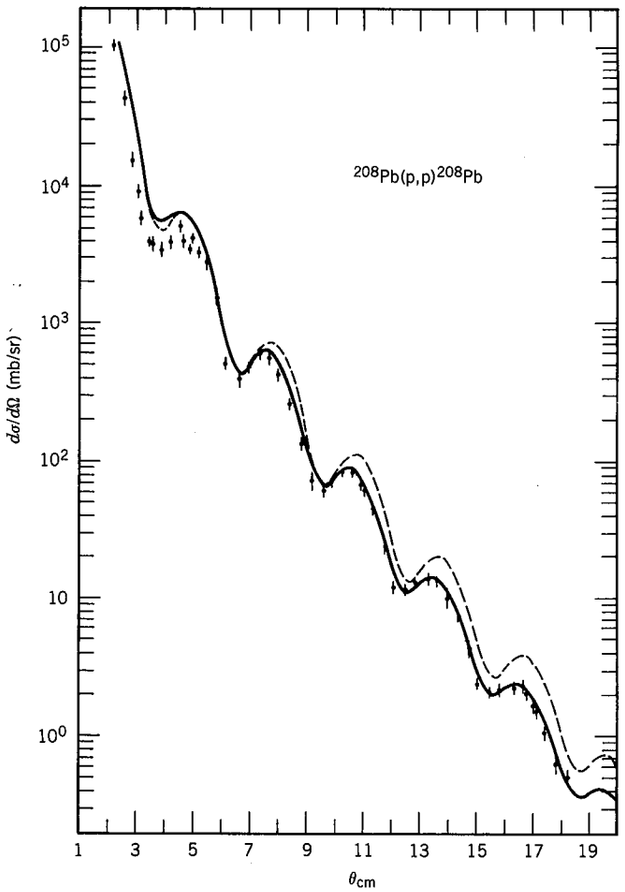

Figure 11.15 Elastic scattering of protons from ^{208}Pb. In (*a*), at low energy (14 MeV), the diffraction-like behavior occurs only at large angles (beyond 60°), where nuclear scattering occurs, because the closest distance between projectile and target (12.6 fm at 60° from the Rutherford formulas) agrees with the internuclear distance appropriate for nuclear interactions (11.8 fm), calculated using $R_0 = 1.7$ fm, as in Figure 11.11. Compare this figure with that for neutron scattering at the same energy, Figure 11.14. In (*b*), the incident energy is 1050 MeV and the Coulomb barrier is easily penetrated, so diffraction effects occur at small angles. (*a*) From J. S. Eck and W. J. Thompson, *Nucl. Phys. A* **237**, 83 (1975). (*b*) From G. Igo, in *High Energy Physics and Nuclear Structure — 1975,* edited by D. Nagle et al. (New York: American Institute of Physics, 1975).

A nucleus is a strongly absorbing object for nucleons, and thus the analogy with the opaque disk is quite valid. For charged particles, we must deal with the interference between nuclear and Coulomb scattering, as in Figure 4.9 and Equation 4.43. It is this effect that is responsible for the deviation of scattering cross sections from the Rutherford formula, as shown in Figure 11.11. If we wish to observe the elastic scattering of nucleons, in the form of the "diffraction-like" pattern, we must eliminate the effects of Rutherford scattering, which we can do in either of two ways. The first is to use uncharged neutrons as the scattered particle. Figure 11.14 shows an example of neutron elastic scattering. One particular difference between the nuclear scattering and optical diffraction is that the minima do not fall to zero. This is a direct result of the diffuseness of the nuclear surface—nuclei do not have sharp edges.

For charged particles, we must take two steps to reduce the effect of interference with Coulomb scattering: we work at higher energy, so that the Rutherford cross section is small and the projectile can more easily penetrate to feel the nuclear interaction, and we observe at larger angles, where again the Rutherford cross section is small and where the small impact parameter also helps to guarantee nuclear penetration. An example of nucleon elastic scattering is shown in Figure 11.15. Again, the diffraction-like effects are apparent.

One result of nucleon elastic scattering studies is the determination of the nuclear radius. Although the value may depend somewhat on the potential model used to analyze the scattering (such as the square well discussed in Chapter 4), the results are generally quite consistent with $R = R_0 A^{1/3}$ with $R_0 = 1.25$ fm as in other studies. In Section 11.9 we discuss in more detail the implication of these experiments on our knowledge of the potential.

Inelastic nuclear scattering, like inelastic Coulomb scattering, results when the target nucleus takes energy from the projectile and reaches excited states. (It is also possible for projectiles to be placed in excited states; we ignore this effect for now.) If we measure the energy distribution of scattered projectiles at a fixed angle, we observe a single elastic peak, which is the highest energy scattered projectile. Each inelastic peak corresponds to a specific excited state of the target nucleus. Figure 11.4 showed an example of inelastic nuclear scattering, and another example is discussed in Section 11.11. From the locations of the inelastic peaks, we can learn the energies of the excited states; from their relative heights we learn the relative cross sections for excitation of each state, which tells us something of the wave function of the excited state. We can also measure an angular distribution of scattered projectiles for any excited state, from which we can learn the spin and parity of the excited states.

11.8 SCATTERING AND REACTION CROSS SECTIONS

In this section we cover some details of reaction cross sections more thoroughly than in our previous discussion in Section 4.2. You may wish to review that discussion before proceeding.

We take the z axis to be the direction of the incident beam and assume it can be represented by a plane wave e^{ikz} corresponding to momentum $p = \hbar k$. The outgoing particles will be represented by spherical waves, and so the manipulations become easier if we express the incident plane wave as a superposition of spherical waves:

$$\psi_{\text{inc}} = Ae^{ikz} = A\sum_{\ell=0}^{\infty} i^{\ell}(2\ell+1)\,j_{\ell}(kr)\,P_{\ell}(\cos\theta) \tag{11.31}$$

where A is an appropriately chosen normalization constant. The radial functions $j_{\ell}(kr)$ are *spherical Bessel functions* which were previously given in Table 2.3; they are solutions to the radial part of the Schrödinger equation, Equation 2.60, in a region far from the target where the nuclear potential vanishes. The angular functions $P_{\ell}(\cos\theta)$ are Legendre polynomials:

$$\begin{aligned} P_0(\cos\theta) &= 1 \\ P_1(\cos\theta) &= \cos\theta \\ P_2(\cos\theta) &= \tfrac{1}{2}(3\cos^2\theta - 1) \end{aligned} \tag{11.32}$$

This expansion of the incident (and eventually, the scattered) wave is called the *partial wave expansion*, with each partial wave corresponding to a specific angular momentum ℓ. Such a procedure is valid if the nuclear potential is assumed to be central. What makes the method useful is that it is often sufficient to consider the effect of the nuclear potential on at most only a few of the lowest partial waves (such as $\ell = 0$ or s-wave nucleon-nucleon scattering discussed in Chapter 4). If the particles of momentum p interact with impact parameter b, then the (semiclassical) relative angular momentum will be

$$\ell\hbar = pb$$

or

$$b = \ell\frac{\hbar}{p} = \ell\frac{\lambda}{2\pi} = \ell\lambda\!\!\!^{-} \tag{11.33}$$

where $\lambda\!\!\!^{-} = \lambda/2\pi$ is called the *reduced* de Broglie wavelength. Incidently, $\lambda\!\!\!^{-} = k^{-1}$.

According to quantum mechanics, ℓ can only be defined in integer units, and thus the semiclassical estimate should be revised somewhat. That is, particles with (semiclassical) angular momenta between $0\hbar$ and $1\hbar$ will interact through impact parameters between 0 and $\lambda\!\!\!^{-}$, and thus effectively over an area (cross section) of at most $\pi\lambda\!\!\!^{-2}$. With $\hbar \le \ell \le 2\hbar$, the cross section is a ring of inner radius $\lambda\!\!\!^{-}$ and outer radius $2\lambda\!\!\!^{-}$, and thus of area $3\pi\lambda\!\!\!^{-2}$. We can thus divide the interaction area into a number of zones, each corresponding to a specific angular momentum ℓ and each having area $\pi[(\ell+1)\lambda\!\!\!^{-}]^2 - \pi(\ell\lambda\!\!\!^{-})^2 = (2\ell+1)\pi\lambda\!\!\!^{-2}$. We can estimate the maximum impact parameter for nuclear scattering to be about $R = R_1 + R_2$ (the sum of the radii of the incident and target nuclei), and thus the maximum ℓ value likely to occur is $R/\lambda\!\!\!^{-}$, and the total cross section is correspondingly

$$\sigma = \sum_{\ell=0}^{R/\lambda\!\!\!^{-}} (2\ell+1)\pi\lambda\!\!\!^{-2} = \pi(R+\lambda\!\!\!^{-})^2 \tag{11.34}$$

This is a reasonable estimate, for it includes not only an interaction distance R, but it allows the incident particle's wave nature to spread over a distance of the order of $\lambda\!\!\!^{-}$, making the effective interaction radius $(R + \lambda\!\!\!^{-})$. We will see later how the exact calculation modifies this estimate.

When the wave is far from the nucleus, the $j_\ell(kr)$ have the following convenient expansion:

$$j_\ell(kr) \cong \frac{\sin\left(kr - \frac{1}{2}\ell\pi\right)}{kr} \qquad (kr \gg \ell)$$

$$= i\frac{e^{-i(kr-\ell\pi/2)} - e^{+i(kr-\ell\pi/2)}}{2kr} \tag{11.35}$$

so that

$$\psi_{\text{inc}} = \frac{A}{2kr}\sum_{\ell=0}^{\infty} i^{\ell+1}(2\ell+1)[e^{-i(kr-\ell\pi/2)} - e^{+i(kr-\ell\pi/2)}]P_\ell(\cos\theta) \tag{11.36}$$

The first term in brackets, involving e^{-ikr}, represents an incoming spherical wave converging on the target, while the second term, in e^{+ikr}, represents an outgoing spherical wave emerging from the target nucleus. The superposition of these two spherical waves, of course, gives the plane wave.

The scattering can affect only the outgoing wave, and can affect it in either of two ways: through a change in phase (as in the phase shift discussed in Chapter 4), and through a change in amplitude. The change in amplitude suggests that there may be fewer particles coming out than there were going in, which may appear to be a loss in the net number of particles. However, keep in mind that the wave function represents only those particles of momentum $\hbar k$. If there is inelastic scattering (or some other nuclear reaction), the energy (or even the identity) of the outgoing particle may change. It is therefore not surprising that there may be fewer particles in the e^{ikr} term following inelastic scattering. It has become customary to refer to a specific set of conditions (exclusive of direction of travel) of the outgoing particle and residual nucleus as a reaction *channel*. The reaction may thus proceed through the elastic channel or through any one of many inelastic channels. Some channels may be *closed* to the reacting particles, if there is not enough energy or angular momentum to permit a specific final configuration to be reached.

We account for the changes in the ℓth outgoing partial wave by introducing the complex coefficient η_ℓ into the outgoing (e^{ikr}) term of Equation 11.36:

$$\psi = \frac{A}{2kr}\sum_{\ell=0}^{\infty} i^{\ell+1}(2\ell+1)\left[e^{-i(kr-\ell\pi/2)} - \eta_\ell e^{+i(kr-\ell\pi/2)}\right]P_\ell(\cos\theta) \tag{11.37}$$

This wave represents a superposition of the incident and scattered waves: $\psi = \psi_{\text{inc}} + \psi_{\text{sc}}$, exactly as in Equation 4.23. To find the scattered wave itself, we subtract Equation 11.37 from Equation 11.36:

$$\psi_{\text{sc}} = \frac{A}{2kr}\sum_{\ell=0}^{\infty} i^{\ell+1}(2\ell+1)(1-\eta_\ell)e^{i(kr-\ell\pi/2)}P_\ell(\cos\theta)$$

$$= \frac{A}{2k}\frac{e^{ikr}}{r}\sum_{\ell=0}^{\infty}(2\ell+1)i(1-\eta_\ell)P_\ell(\cos\theta) \tag{11.38}$$

Because we have accounted for only those parts of ψ_{sc} with wave number k identical with the incident wave, this represents only *elastic scattering*. As we did in Equation 4.24 we now find the scattered current density:

$$j_{\text{sc}} = \frac{\hbar}{2mi}\left(\psi_{\text{sc}}^*\frac{\partial\psi_{\text{sc}}}{\partial r} - \frac{\partial\psi_{\text{sc}}^*}{\partial r}\psi_{\text{sc}}\right) \tag{11.39}$$

$$= |A|^2\frac{\hbar}{4mkr^2}\left|\sum_{\ell=0}^{\infty}(2\ell+1)i(1-\eta_\ell)P_\ell(\cos\theta)\right|^2 \tag{11.40}$$

The incident current is identical with Equation 4.26:

$$j_{\text{inc}} = \frac{\hbar k}{m}|A|^2 \tag{11.41}$$

and by analogy with Equation 4.27, the differential cross section is

$$\frac{d\sigma}{d\Omega} = \frac{1}{4k^2}\left|\sum_{\ell=0}^{\infty}(2\ell+1)i(1-\eta_\ell)P_\ell(\cos\theta)\right|^2 \tag{11.42}$$

To find the total cross section, we require the integral of the Legendre polynomials:

$$\int P_\ell(\cos\theta)P_{\ell'}(\cos\theta)\sin\theta\,d\theta\,d\phi = \frac{4\pi}{2\ell+1} \qquad \text{if } \ell = \ell'$$

$$= 0 \qquad \text{if } \ell \neq \ell' \tag{11.43}$$

Thus

$$\sigma_{\text{sc}} = \sum_{\ell=0}^{\infty}\pi\lambda\!\!\!^{-2}(2\ell+1)|1-\eta_\ell|^2 \tag{11.44}$$

If elastic scattering were the only process that could occur, then $|\eta_\ell| = 1$ and it is conventional to write $\eta_\ell = e^{2i\delta_\ell}$ where δ_ℓ is the *phase shift* of the ℓth partial wave. For this case, $|1-\eta_\ell|^2 = 4\sin^2\delta_\ell$ and

$$\sigma_{\text{sc}} = \sum_{\ell=0}^{\infty}4\pi\lambda\!\!\!^{-2}(2\ell+1)\sin^2\delta_\ell \tag{11.45}$$

which reduces directly to Equation 4.30 for $\ell = 0$.

If there are other processes in addition to elastic scattering (inelastic scattering or other reactions) then Equation 11.45 is not valid, because $|\eta_\ell| < 1$. We group all of these processes together under the term *reaction cross section* σ_r, where we take "reaction" to mean all nuclear processes *except* elastic scattering. To find this cross section, we must examine Equation 11.37 to find the rate at which particles are "disappearing" from the channel with wave number k. That is, we find the difference between the incoming current and the outgoing current using,

respectively, the first and second terms of Equation 11.37:

$$|j_{in}| - |j_{out}| = \frac{|A|^2\hbar}{4mkr^2}\left\{\left|\sum_{\ell=0}^{\infty}(2\ell+1)i^{\ell+1}e^{i\ell\pi/2}P_\ell(\cos\theta)\right|^2 - \left|\sum_{\ell=0}^{\infty}(2\ell+1)i^{\ell+1}\eta_\ell e^{-i\ell\pi/2}P_\ell(\cos\theta)\right|^2\right\} \quad (11.46)$$

and the reaction cross section becomes

$$\sigma_r = \sum_{\ell=0}^{\infty}\pi\lambda\!\!\!^{-2}(2\ell+1)(1-|\eta_\ell|^2) \quad (11.47)$$

The *total* cross section, including all processes, is

$$\sigma_t = \sigma_{sc} + \sigma_r = \sum_{\ell=0}^{\infty}2\pi\lambda\!\!\!^{-2}(2\ell+1)(1-\operatorname{Re}\eta_\ell) \quad (11.48)$$

You should note the following details about these results:

1. It is possible to have elastic scattering in the absence of other processes; that is, if $|\eta_\ell| = 1$, then Equation 11.47 vanishes. It is *not* possible, however, to have reactions without also having elastic scattering; that is, any choice of η_ℓ for which $\sigma_r \neq 0$ for a given partial wave automatically gives $\sigma_{sc} \neq 0$ for that partial wave. We can understand this with reference to the diffraction model of scattering we considered in Section 11.7. If particles are removed from the incident beam, creating a "shadow" behind the target nucleus, incident particles will be diffracted into the shadow.
2. For a "black disk" absorber, as in Equation 11.34, in which all partial waves are completely absorbed up to $\ell = R/\lambda\!\!\!^{-}$ ($\eta_\ell = 0$ for complete absorption) and unaffected for $\ell > R/\lambda\!\!\!^{-}$ ($\eta_\ell = 1$), then

$$\sigma_{sc} = \pi(R + \lambda\!\!\!^{-})^2 \quad (11.49)$$

and

$$\sigma_r = \pi(R + \lambda\!\!\!^{-})^2 \quad (11:50)$$

so that

$$\sigma_t = 2\pi(R + \lambda\!\!\!^{-})^2 \quad (11.51)$$

The total cross section is *twice* the geometrical area! The explanation for this nonclassical effect can also be found in the "shadow" region—the target nucleus cannot simply absorb and throw a sharp shadow. It must also diffract into the shadow region.

The program for using these results to study nuclear structure is similar to that of Chapter 4 for nucleon–nucleon scattering. We can guess at a form for the nuclear potential, solve the Schrödinger equation inside the interaction region

$0 \leq r \leq R$, and match boundary conditions at the surface. In this way we should be able to calculate η_ℓ and, by comparison with experimental values of σ_{sc} and σ_r, evaluate whether our chosen form for the potential is reasonable. In practice this is very difficult for all but the elastic channel because all of the inelastic and reaction channels are coupled together leading to a complicated system of coupled equations. We discuss one particular technique, the optical model for elastic scattering, in Section 11.9.

11.9 THE OPTICAL MODEL

A simple model used to account in a general way for elastic scattering in the presence of absorptive effects is the *optical model*, so called because the calculation resembles that of light incident on a somewhat opaque glass sphere. (The model is also called the "cloudy crystal ball model.")

In this model, we represent the scattering in terms of a complex potential $U(r)$:

$$U(r) = V(r) + iW(r) \quad (11.52)$$

where the real functions V and W are selected to give the potential its proper radial dependence. The real part, $V(r)$, is responsible for the elastic scattering; it describes the ordinary nuclear interaction between target and projectile and may therefore be very similar to a shell-model potential. The imaginary part, $W(r)$, is responsible for the absorption. We can demonstrate this by considering a square-well form for $U(r)$:

$$\begin{aligned} U(r) &= -V_0 - iW_0 \qquad r < R \\ &= 0 \qquad\qquad\quad r > R \end{aligned} \quad (11.53)$$

The outgoing scattered wave we take to be in the form of e^{ikr}/r, with $k = \sqrt{2m(E + V_0 + iW_0)/\hbar^2}$, which follows from solving the Schrödinger equation in the usual way for this potential. The wave number k is thus complex: $k = k_r + ik_i$, where k_r and k_i are the real and imaginary parts, respectively. The wave function behaves like $e^{ik_r r} \cdot e^{-k_i r}/r$, and the radial probability density is proportional to $e^{-2k_i r}$. The wave is therefore exponentially attenuated as it passes through the nucleus. (Choosing $W_0 > 0$ in Equation 11.53 gives a loss in intensity, rather than a gain.) If we assume that the absorption is relatively weak (that is, W_0 is small compared with $E + V_0$), then we can use the binomial theorem to expand the expression for k:

$$k \cong \sqrt{\frac{2m(E+V_0)}{\hbar^2}} + \frac{iW_0}{2}\sqrt{\frac{2m}{\hbar^2}\left(\frac{1}{E+V_0}\right)} \quad (11.54)$$

The usual shell-model potential has a depth V_0 of the order of 40 MeV, and we can take $E = 10$ MeV for a typical low-energy projectile. The distance over which the intensity is attenuated by e^{-1} (a sort of mean free path) is

$$d = \frac{1}{2k_i} = \frac{1}{W_0}\sqrt{\frac{\hbar^2(E+V_0)}{2m}} \quad (11.55)$$

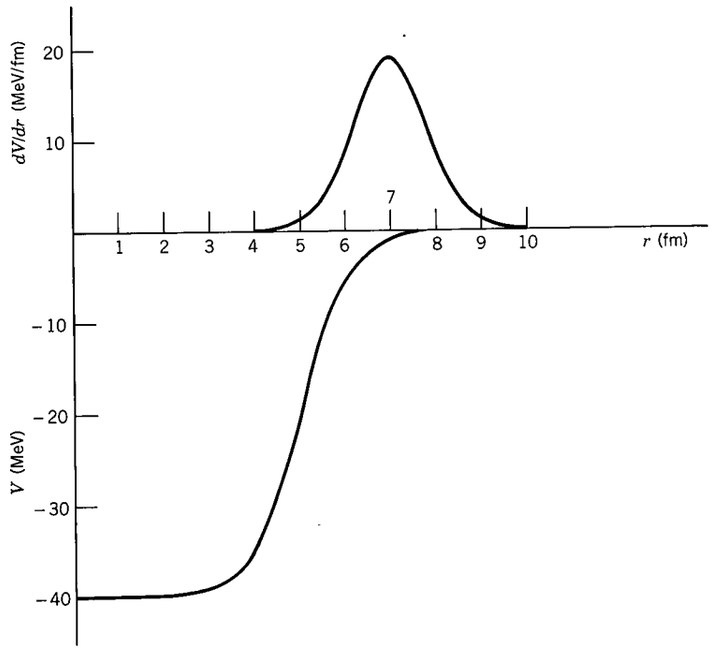

Figure 11.16 The optical model functions $V(r)$ and $W(r) = dV/dr$. Typical parameters chosen are $V_0 = 40$ MeV, $R = 1.25A^{1/3}$, $a = 0.523$ fm, and $A = 64$.

If this distance is to be at most of the order of the nuclear radius (say, 3 fm) then $W_0 \simeq 11$ MeV. Thus for the usual case, in which absorption is relatively weaker than elastic scattering, we estimate $|V| \sim 40$ MeV, $|W| \sim 10$ MeV.

The procedure for applying the optical model might be as follows: First, we must choose a form for the potential. The square-well form is often adequate (with $R \simeq 1.4A^{1/3}$, a bit larger than usual to account for the diffuse nuclear surface), but a more detailed form is often chosen:

$$V(r) = \frac{-V_0}{1 + e^{(r-R)/a}} \tag{11.56}$$

exactly as in the case of the shell model, Equation 5.1. The constants V_0, R, and a are adjusted to give the best fits with the scattering data. The absorptive part $W(r)$ at low energies must have a very different form. Because of the exclusion principle, the tightly bound nucleons in the nuclear interior cannot participate in absorbing incident nucleons. Only the "valence" nucleons near the surface can absorb the relatively low energy carried by the incident particle. The function $W(r)$ is thus often chosen as proportional to dV/dr, which has the proper shape of being large only near the surface, as shown in Figure 11.16. (At higher energy, where the inner nucleons can also participate in absorption, $W(r)$ may look more like $V(r)$.) A *spin-orbit* term is also included in modern optical potentials. It is also peaked near the surface, because the spin density of the inner nucleons vanishes. Finally, a Coulomb term must be included if the incident particle is

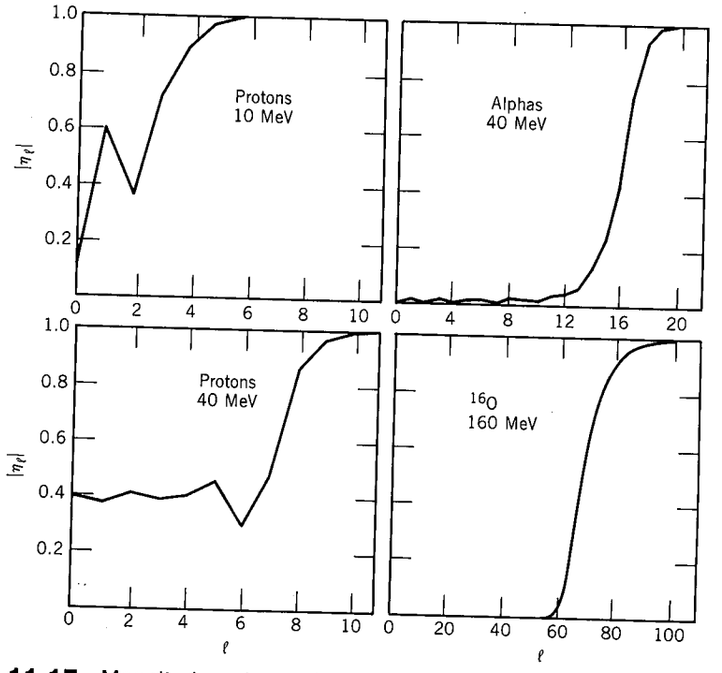

Figure 11.17 Magnitudes of complex scattering amplitudes η_ℓ for scattering of various projectiles on a target of ^{58}Ni. The approach of $|\eta_\ell|$ to 1 at higher energy corresponds to $\sigma_r \to 0$, so that few particles are absorbed and only elastic scattering takes place. From G. R. Satchler, *Introduction to Nuclear Reactions* (Wiley: New York, 1980).

charged. For the chosen potential, the Schrödinger equation can be solved, and equating boundary conditions at $r = R$, as we did in Chapter 4 for the nucleon-nucleon problem, gives the complex scattering amplitudes η_ℓ, which can be used to compare calculated cross sections with experiment. Figure 11.17 shows examples of some η_ℓ values.

The complete optical model fits to scattering data often are very impressive. Figure 11.18 shows an example of several fits to elastic scattering cross sections and polarizations.

The optical model is useful only in discussing average behavior in reactions such as scattering. Many of the interesting features of the microscopic structure of nuclei are accounted for indirectly only in this average way. The calculation using the optical model, as described in this section, does not deal with where the absorbed particles actually go; they simply disappear from the elastic channel. In fact, the many interactions between the nucleons of the target and projectile are so complicated that representing them by a single potential is itself a significant approximation. Nevertheless, the optical model is successful in accounting for elastic and inelastic scattering and leads us to an understanding of the interactions of nuclei.

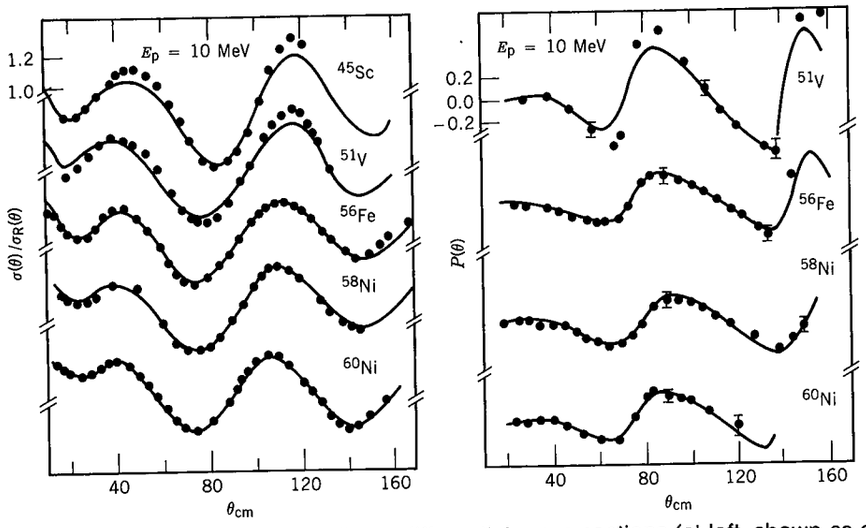

Figure 11.18 Optical-model fits to differential cross sections (at left, shown as a ratio to the Rutherford cross section) and polarizations, for 10-MeV protons scattered elastically from various targets. The solid lines are the fits to the data using the best set of optical-model parameters. From F. D. Becchetti, Jr., and G. W. Greenlees, *Phys. Rev.* **182**, 1190 (1969).

11.10 COMPOUND-NUCLEUS REACTIONS

Suppose an incident particle enters a target nucleus with an impact parameter small compared with the nuclear radius. It then will have a high probability of interacting with one of the nucleons of the target, possibly through a simple scattering. The recoiling struck nucleon and the incident particle (now with less energy) can each make successive collisions with other nucleons, and after several such interactions, the incident energy is shared among many of the nucleons of the combined system of projectile + target. The average increase in energy of any single nucleon is not enough to free it from the nucleus, but as many more-or-less random collisions occur, there is a statistical distribution in energies and a small probability for a single nucleon to gain a large enough share of the energy to escape, much as molecules evaporate from a hot liquid.

Such reactions have a definite intermediate state, after the absorption of the incident particle but before the emission of the outgoing particle (or particles). This intermediate state is called the *compound nucleus*. Symbolically then the reaction a + X → Y + b becomes

$$a + X \rightarrow C^* \rightarrow Y + b$$

where C* indicates the compound nucleus.

As might be assumed from seeing the reaction written in this form, we can consider a reaction that proceeds through the compound nucleus to be a two-step process: the formation and then the subsequent decay of the compound nucleus. A given compound nucleus may decay in a variety of different ways, and essential to the compound-nucleus model of nuclear reactions is the assumption that *the*

relative probability for decay into any specific set of final products is independent of the means of formation of the compound nucleus. The decay probability depends only on the total energy given to the system; in effect, the compound nucleus "forgets" the process of formation and decays governed primarily by statistical rules.

Let's consider a specific example. The compound nucleus $^{64}Zn^*$ can be formed through several reaction processes, including $p + {}^{63}Cu$ and $\alpha + {}^{60}Ni$. It can also decay in a variety of ways, including $^{63}Zn + n$, $^{62}Zn + 2n$, and $^{62}Cu + p + n$. That is

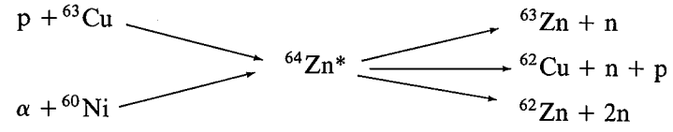

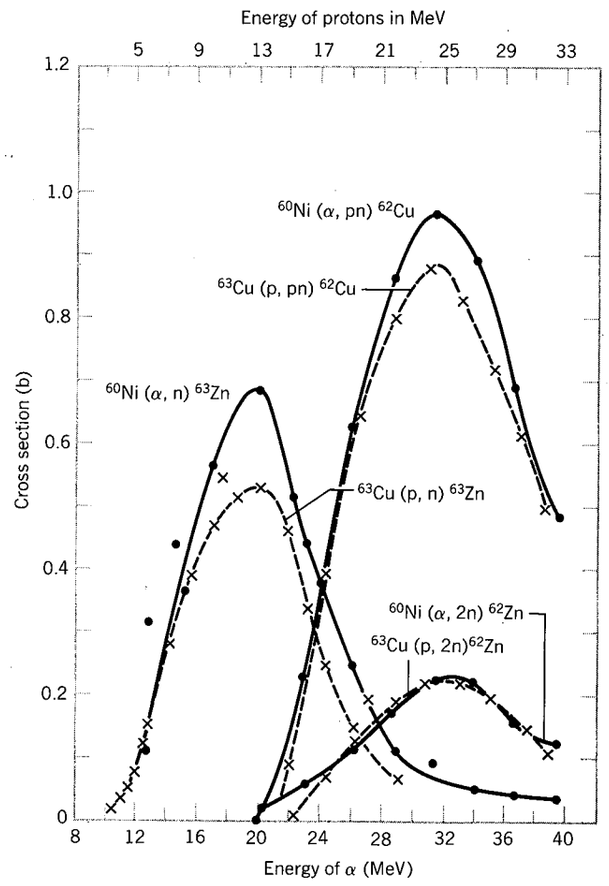

Figure 11.19 Cross sections for different reactions leading to the compound nucleus ^{64}Zn show very similar characteristics, consistent with the basic assumptions of the compound nucleus model. From S. N. Goshal, *Phys. Rev.* **80**, 939 (1950).

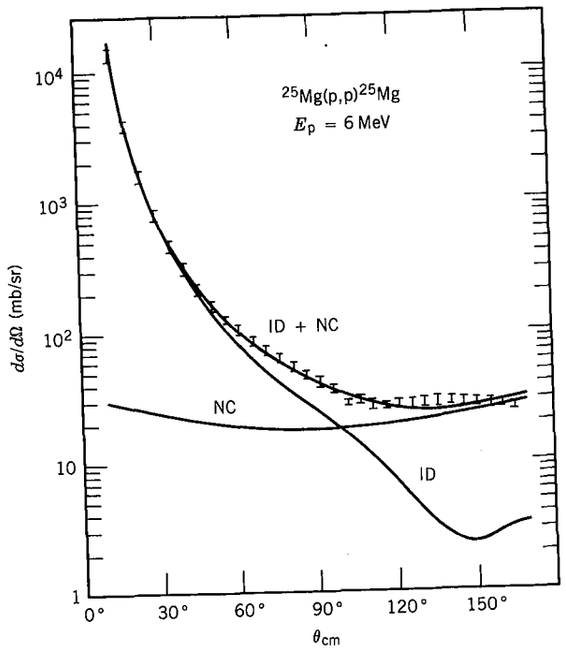

Figure 11.20 The curve marked NC shows the contribution from compound-nucleus formation to the cross section of the reaction ^{25}Mg(p, p)^{25}Mg. The curve marked ID shows the contribution from direct reactions. Note that the direct part has a strong angular dependence, while the compound-nucleus part shows little angular dependence. From A. Gallmann et al., *Nucl. Phys.* **88**, 654 (1966).

If this model were correct, we would expect for example that the relative cross sections for ^{63}Cu(p, n)^{63}Zn and ^{60}Ni(α, n)^{63}Zn would be the same at incident energies that give the same excitation energy to ^{64}Zn*. Figure 11.19 shows the cross sections for the three final states, with the energy scales for the incident protons and α's shifted so that they correspond to a common excitation of the compound nucleus. The agreement between the three pairs of cross sections is remarkably good, showing that indeed, the decay of ^{64}Zn* into any specific final state is nearly independent of how it was originally formed.

The compound-nucleus model works best for low incident energies (10–20 MeV), where the incident projectile has a small chance of escaping from the nucleus with its identity and most of its energy intact. It also works best for medium-weight and heavy nuclei, where the nuclear interior is large enough to absorb the incident energy.

Another characteristic of compound-nucleus reactions is the angular distribution of the products. Because of the random interactions among the nucleons, we expect the outgoing particle to be emitted with a nearly isotropic angular distribution (that is, the same in all directions). This expectation is quite consistent with experiment, as shown in Figure 11.20. In cases in which a heavy ion is the incident particle, large amounts of angular momentum can be transferred to the compound nucleus, and to extract that angular momentum the

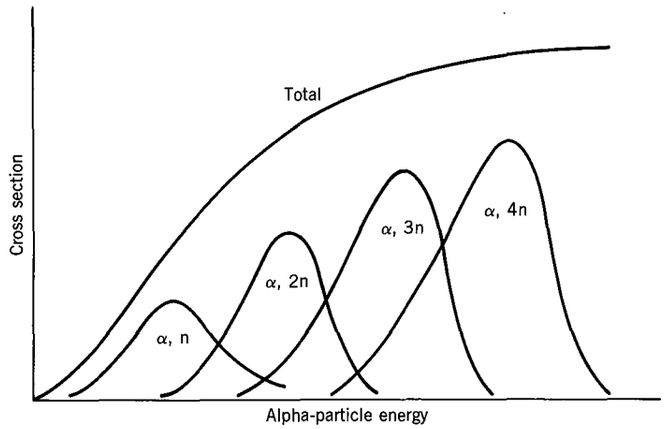

Figure 11.21 At higher incident energies, it is more likely that additional neutrons will "evaporate" from the compound nucleus.

emitted particles tend to be emitted at right angles to the angular momentum, and thus preferentially at 0 and 180°. With light projectiles, this effect is negligible.

The "evaporation" analogy mentioned previously is really quite appropriate. In fact, the more energy we give to the compound nucleus, the more particles are likely to evaporate. For each final state, the cross section has the Gaussian-like shape shown in Figure 11.19. Figure 11.21 shows the cross sections for (α, xn) reactions, where $x = 1, 2, 3, \ldots$. For each reaction, the cross section increases to a maximum and then decreases as the higher energy makes it more likely for an additional neutron to be emitted.

11.11 DIRECT REACTIONS

At the opposite extreme from compound-nucleus reactions are *direct* reactions, in which the incident particle interacts primarily at the surface of the target nucleus; such reactions are also called *peripheral* processes. As the energy of the incident particle is increased, its de Broglie wavelength decreases, until it becomes more likely to interact with a nucleon-sized object than with a nucleus-sized object. A 1-MeV incident nucleon has a de Broglie wavelength of about 4 fm, and thus does not "see" individual nucleons; it is more likely to interact through a compound-nucleus reaction. A 20-MeV nucleon has a de Broglie wavelength of about 1 fm and therefore may be able to participate in direct processes. Direct processes are most likely to involve one nucleon or very few valence nucleons near the surface of the target nucleus.

Of course, it may be possible to have direct and compound-nucleus processes both contribute to a given reaction. How can we distinguish their contributions or decide which may be more important? There are two principal differences that can be observed experimentally: (1) Direct processes occur very rapidly, in a time of the order of 10^{-22} s, while compound-nuclear processes typically take much longer, perhaps 10^{-16} to 10^{-18} s. This additional time is necessary for the

distribution and reconcentration of the incident energy. There are ingenious experimental techniques for distinguishing between these two incredibly short intervals of time. (2) The angular distributions of the outgoing particles in direct reactions tend to be more sharply peaked than in the case of compound-nuclear reactions.

Inelastic scattering could proceed either through a direct process or a compound nucleus, largely depending on the energy of the incident particle. The *deuteron stripping reaction* (d, n), which is an example of a *transfer reaction* in which a single proton is transferred from projectile to target, may also go by either mechanism. Another deuteron stripping reaction (d, p) may be more likely to go by a direct process, for the "evaporation" of protons from the compound nucleus is inhibited by the Coulomb barrier. The (α, n) reaction is less likely to be a direct process, for it would involve a single transfer of three nucleons into valence states of the target, a highly improbable process.

One particularly important application of single-particle transfer reactions, especially (d, p) and (d, n), is the study of low-lying shell-model excited states. Several such states may be populated in a given reaction; we can choose a particular excited state from the energy of the outgoing nucleon. Once we have done so, we would like to determine just which shell-model state it is. For this we need the angular distribution of the emitted particles, which often give the spin and parity of the state that is populated in a particular reaction. Angular distributions therefore are of critical importance in studies of transfer reactions. (*Pickup reactions*, for example (p, d), in which the projectile takes a nucleon from the target, also give information on single-particle states.)

Let's consider in somewhat more detail the angular momentum transfer in a deuteron stripping reaction. In the geometry of Figure 11.22, an incident particle with momentum $\boldsymbol{p}_a$ gives an outgoing particle with momentum $\boldsymbol{p}_b$, while the residual nucleus (target nucleus plus transferred nucleon) must recoil with momentum $\boldsymbol{p} = \boldsymbol{p}_a - \boldsymbol{p}_b$. In a direct process, we may assume that the transferred nucleon instantaneously has the recoil momentum and that it must be placed in an orbit with orbital angular momentum $\ell = Rp$, assuming that the interaction

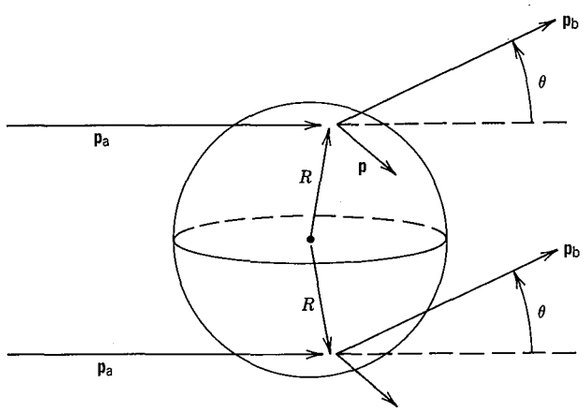

Figure 11.22 Geometry for direct reactions occurring primarily on the nuclear surface.

takes place at the surface of the nucleus. The momentum vectors are related by the law of cosines:

$$p^2 = p_a^2 + p_b^2 - 2p_a p_b \cos\theta$$
$$= (p_a - p_b)^2 + 2p_a p_b(1 - \cos\theta) \qquad (11.57)$$

Given the energies of the incident and outgoing particles, we then have a direct relationship between ℓ and θ—particles emerging at a given angle should correspond to a specific angular momentum of the orbiting particle.

Consider a specific example, the (d, p) reaction on ^{90}Zr leading to single neutron shell-model states in ^{91}Zr. The Q value is about 5 MeV, so an incident deuteron at 5 MeV gives a proton at about 10 MeV, less any excitation in ^{91}Zr. Since at these energies $p_a \simeq p_b \simeq 140$ MeV/c, Equation 11.57 gives

$$\ell = \left[\frac{2c^2 p_a p_b(2\sin^2\theta/2)}{\hbar^2 c^2/R^2}\right]^{1/2} \cong 8\sin\frac{\theta}{2}$$

For each angular momentum transfer, we expect to find outgoing protons at the following angles: $\ell = 0$, 0°; $\ell = 1$, 14°; $\ell = 2$, 29°; $\ell = 3$, 44°.

This simple semiclassical estimate will be changed by the intrinsic spins of the particles, which we neglected. There will also be interference between scatterings that occur on opposite sides of the nucleus, as shown in Figure 11.22. These interferences result in maxima and minima in the angular distributions.

Figure 11.23 shows the result of studies of (d, p) reactions on ^{90}Zr. You can see several low-lying states in the proton spectrum, and from their angular distributions we can assign them to specific spins and parities in ^{91}Zr. Notice the appearance of maxima and minima in the angular distribution. The angular momentum transfer, as usual, also gives us the change in parity of the reactions, ℓ = even for no change in parity and ℓ = odd for a change in parity. If we are studying shell-model states in odd-A nuclei by single-particle transfer reactions such as (d, p), we will use an even-Z, even-N nucleus as target, and so the initial spin and parity are 0^+. If the orbital angular momentum transferred is ℓ, then the final nuclear state reached will be $\ell \pm \frac{1}{2}$, allowing for the contribution of the spin of the transferred nucleon. For $\ell = 2$, for instance, we can reach states of $j = \frac{3}{2}$ or $\frac{5}{2}$, both with even parity.

The complete theory of direct reactions is far too detailed for this text, but we can sketch the outline of the calculation as an exercise in applications of the principles of quantum mechanics. The transition amplitude for the system to go from the initial state (X + a) to the final state (Y + b) is governed by the usual quantum mechanical matrix element:

$$M = \int \psi_Y^* \psi_b^* V \psi_X \psi_a \, dv \qquad (11.58)$$

The interaction V must be a very complicated function of many nuclear coordinates. A simplifying assumption is the plane-wave *Born approximation*, in which ψ_a and ψ_b are treated as plane waves. Expanding the resulting exponential $e^{i\boldsymbol{p}\cdot\boldsymbol{r}/\hbar}$ using a spherical wave expansion of the form of Equation 11.31 and making the simplifying assumption that the interaction takes place on the nuclear

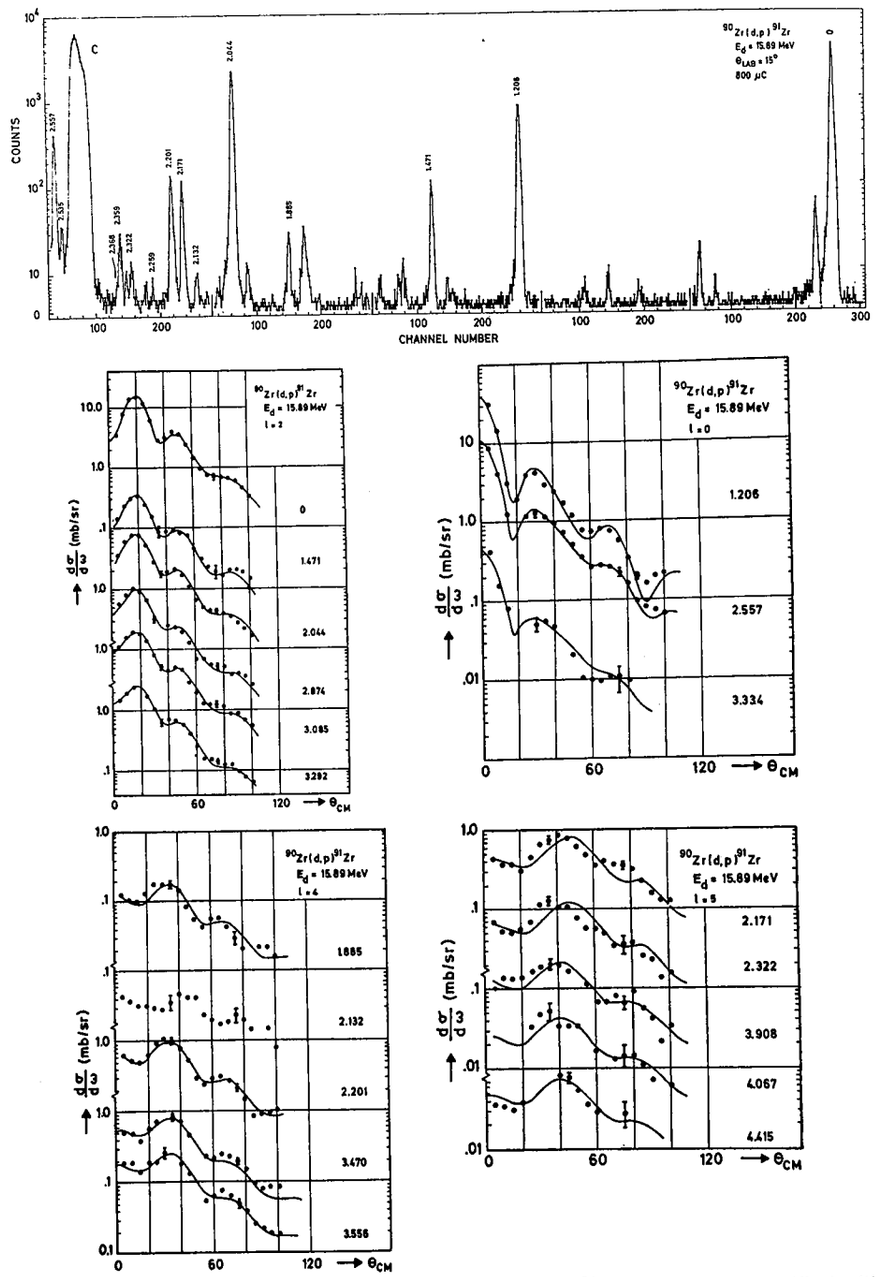

Figure 11.23 (top) Proton spectrum from ^{90}Zr(d, p)^{91}Zr. Peaks are identified with the final states in ^{91}Zr populated. The large peak at the left is from a carbon impurity. (bottom) Angular distributions fitted to determine the ℓ value. Note that the location of the first maximum shifts to larger angles with increasing ℓ, as predicted by Equation 11.57. See Figure 11.24 for the deduced excited states. Data from H. P. Blok et al., *Nucl. Phys. A* **273**, 142 (1976).

surface, so the integral is evaluated only at $r = R$, the matrix element is proportional to $j_\ell(kR)$ where $k = p/\hbar$ contains the explicit angular dependence through Equation 11.57. The cross section then depends on $[j_\ell(kR)]^2$, which gives results of the form of Figure 11.23.

Taking this calculation one step further, we use the optical model to account for the fact that the incoming and outgoing plane waves are changed (or distorted) by the nucleus. This gives the *distorted-wave Born approximation*, or DWBA. We can even put in explicit shell-model wave functions for the final state, and ultimately we find a differential cross section for the reaction. Because there are no "pure" shell-model states, the calculated cross section may describe many different final states. Each will have a differential cross section whose shape can be accurately calculated based on this model, but the amplitude of the cross section for any particular state depends on the fraction of the pure shell-model state included in the wave function for that state. The measured cross section is thus reduced from the calculated shell-model single-particle value by a number

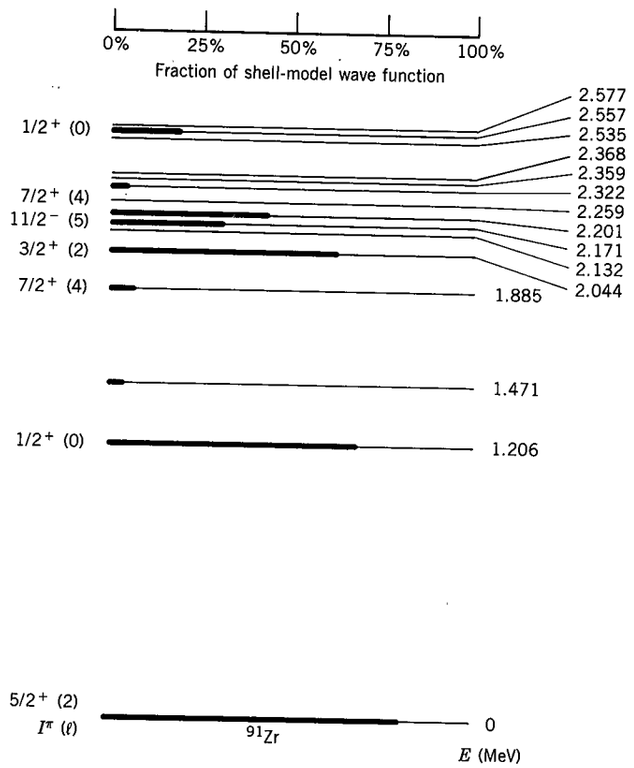

Figure 11.24 Deduced level scheme for ^{91}Zr. Each ℓ value (except zero) deduced from the angular distributions of Figure 11.23 leads to a definite parity assignment but to two possible I values, $\ell \pm \frac{1}{2}$. Which one is correct must be determined from other experiments. The fraction of the single-particle strengths represented by each level is indicated by the length of the shading; thus the ground state is nearly pure $d_{5/2}$ shell-model state.

between 0 and 1 called the *spectroscopic factor* S:

$$\left(\frac{d\sigma}{d\Omega}\right)_{\text{meas}} = S\left(\frac{d\sigma}{d\Omega}\right)_{\text{calc}} \tag{11.59}$$

A pure shell-model state would have $S = 1$. In practice we often find the shell-model wave function to be distributed over many states. Figure 11.24 shows examples of the spectroscopic factors measured for ^{91}Zr.

11.12 RESONANCE REACTIONS

The compound-nucleus model of nuclear reactions treats the unbound nuclear states as if they formed a structureless continuum. That is, there may be discrete nuclear states, but there are so many of them and they are so close together that they form a continuous spectrum. Each of these supposed discrete states is unstable against decay and therefore has a certain *width*; when the states are so numerous that their spacing is much less than the widths of the individual states, the compound-nucleus continuum results.

The bound states studied by direct reactions are at the opposite end of the scale. Because they are stable against particle emission, their mean lives are much longer (for example, characteristic of γ decay) and their corresponding widths are much smaller. A state with a lifetime of 1 ps, for instance, has a width of about 10^{-3} eV, far smaller than the typical spacing of bound states. We are therefore justified in treating these as discrete states with definite wavefunctions.

Between these two extremes is the *resonance* region—discrete levels in the compound-nucleus region. These levels have a high probability of formation (large cross sections), and their widths are very small because at low incident energy, where these resonances are most likely to occur, the quasibound state that is formed usually has only two modes of decay available to it—re-ejecting the incident particle, as in elastic or inelastic scattering, or γ emission.

To obtain a qualitative understanding of the formation of resonances, we represent the nuclear potential seen by the captured particle as a square well. The oscillatory wave functions inside and outside the well must be matched smoothly, as we did in Figure 4.7*a* for nucleon-nucleon scattering. Figure 11.25 shows several examples of how this might occur. Depending on the phase of the wave function inside the nucleus, the smooth matching can result in substantial variations between the relative amplitudes of the wave functions inside and outside the nucleus. In case (a), the incident particle has relatively little probability to penetrate the nucleus and form a quasibound state; in case (c), there is a very high probability to penetrate. As we vary the energy of the incident particle, we vary the relative phase of the inner and outer wave functions; the location of the matching point *and* the relative amplitudes vary accordingly. Only for certain incident energies do we achieve the conditions shown in part (c) of Figure 11.25. These are the energies of the *resonances* in the cross section.

In a single, isolated resonance of energy E_R and width Γ, the energy profile of the cross section in the vicinity of the resonance will have the character of the energy distribution of any decaying state of lifetime $\tau = \hbar/\Gamma$; see, for example, Equation 6.20 or Figure 6.3. The resonance will occur where the total cross

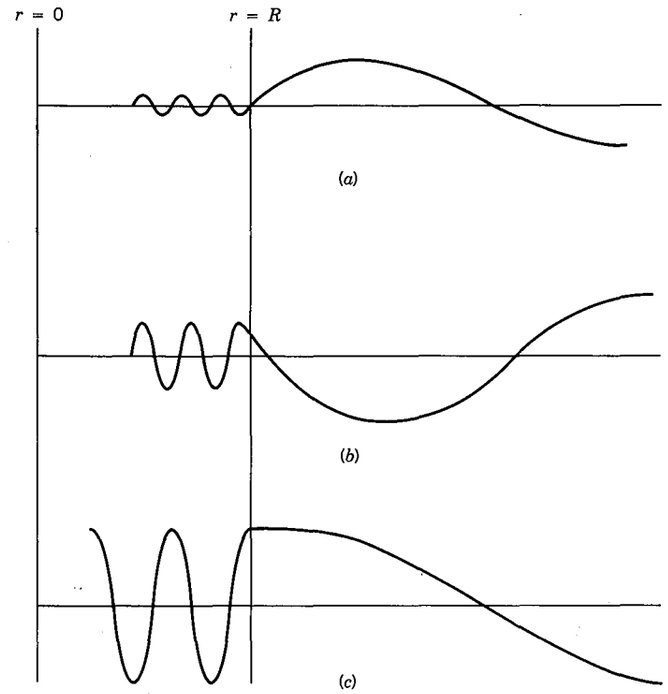

Figure 11.25 (a) Far from resonance, the exterior and interior wave functions match badly, and little penetration of the nucleus occurs. (b) As the match improves, there is a higher probability to penetrate. (c) At resonance the amplitudes match exactly, the incident particle penetrates easily, and the cross section rises to a maximum.

section has a maximum; from Equation 11.48, assuming only one partial wave ℓ is important for the resonant state, there will be a scattering resonance where $\eta_\ell = -1$, corresponding to a phase shift $\delta_\ell = \pi/2$.

The shape of the resonance can be obtained by expanding the phase shift about the value $\delta_\ell = \pi/2$. Better convergence of the Taylor series expansion is obtained if we expand the cotangent of δ_ℓ:

$$\cot \delta_\ell(E) = \cot \delta_\ell(E_R) + (E - E_R)\left(\frac{\partial \cot \delta_\ell}{\partial E}\right)_{E=E_R} + \tfrac{1}{2}(E - E_R)^2\left(\frac{\partial^2 \cot \delta_\ell}{\partial E^2}\right)_{E=E_R} + \cdots \tag{11.60}$$

in which

$$\left(\frac{\partial \cot \delta_\ell}{\partial E}\right)_{E=E_R} = -\left(\frac{\partial \delta_\ell}{\partial E}\right)_{E=E_R} \tag{11.61}$$

Defining the width Γ as

$$\Gamma = 2\left(\frac{\partial \delta_\ell}{\partial E}\right)^{-1}_{E=E_R} \tag{11.62}$$

then it can be shown that the second-order term vanishes, and thus (neglecting higher-order terms)

$$\cot \delta_\ell = -\frac{(E - E_R)}{\Gamma/2} \tag{11.63}$$

Because Γ is the full width of the resonance, the cross section should fall to half of the central value at $E - E_R = \pm\Gamma/2$. From Equation 11.63, this occurs when $\cot \delta_\ell = \pm 1$, or $\delta_\ell = \pi/4, 3\pi/4$ (compared with $\delta_\ell = \pi/2$ at the center of the resonance). The cross section depends on $\sin^2 \delta_\ell$, which does indeed fall to half the central value at $\delta_\ell = \pi/4$ and $3\pi/4$. The width defined by Equation 11.62 is thus entirely consistent with the width shown in Figure 6.3.

From Equation 11.63, we find

$$\sin \delta_\ell = \frac{\Gamma/2}{\left[(E - E_R)^2 + \Gamma^2/4\right]^{1/2}} \tag{11.64}$$

and the scattering cross section becomes, using Equation 11.45

$$\sigma_{sc} = \frac{\pi}{k^2}(2\ell + 1)\frac{\Gamma^2}{(E - E_R)^2 + \Gamma^2/4} \tag{11.65}$$

This result can be generalized in two ways. In the first place, we can account for the effect of reacting particles with spin. If s_a and s_X are the spins of the incident and target particles, and if I is the total angular momentum of the resonance,

$$\boldsymbol{I} = \boldsymbol{s}_a + \boldsymbol{s}_X + \boldsymbol{\ell} \tag{11.66}$$

then the factor $(2\ell + 1)$ in Equation 11.65 should be replaced by the more general statistical factor

$$g = \frac{2I + 1}{(2s_a + 1)(2s_X + 1)} \tag{11.67}$$

Note that g reduces to $(2\ell + 1)$ for spinless particles.

The second change we must make is to allow for partial entrance and exit widths. If the resonance has many ways to decay, then the total width Γ is the sum of all the partial widths Γ_i

$$\Gamma = \sum_i \Gamma_i \tag{11.68}$$

The Γ^2 factor in the denominator of Equation 11.65 is related to the decay width of the resonant state and therefore to its lifetime: $\Gamma = \hbar/\tau$. The observation of only a single entrance or exit channel does not affect this factor, for the resonance always decays with the same lifetime τ. In the analogous situation in

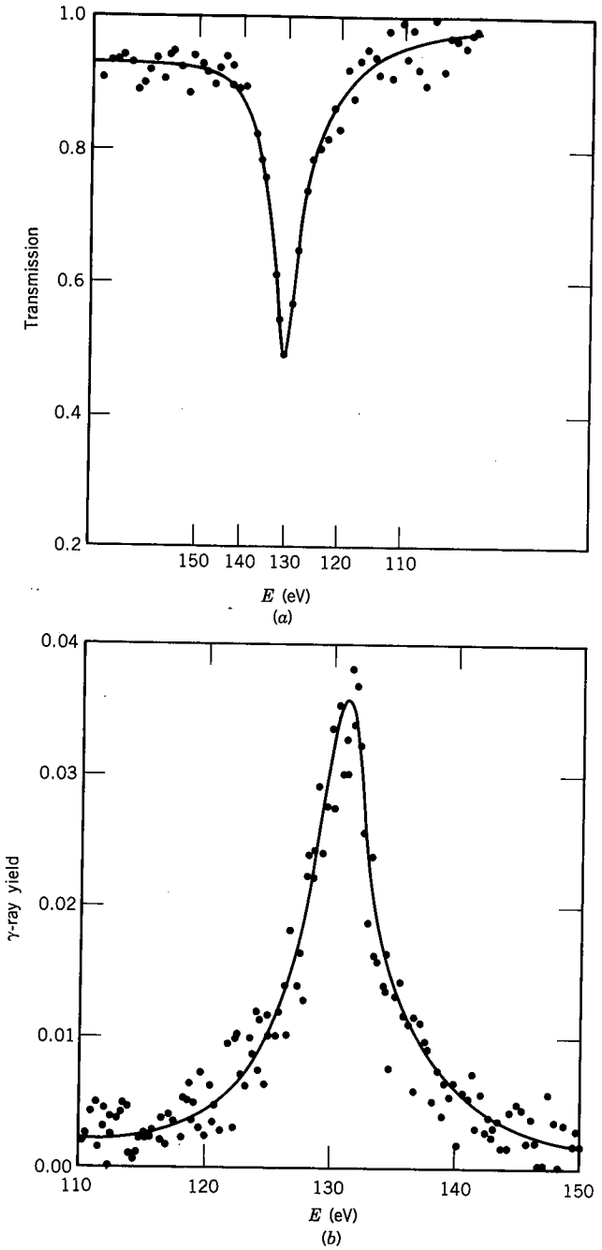

Figure 11.26 130-eV neutron resonance in scattering from ^{59}Co. Part (*a*) shows the intensity of neutrons transmitted through a target of ^{59}Co; at the resonance there is the highest probability for a reaction and the intensity of the transmitted beam drops to a minimum. In (*b*), the γ-ray yield is shown for neutron radiative capture by ^{59}Co. Here the yield of γ rays is maximum where the reaction has the largest probability. From J. E. Lynn, *The Theory of Neutron Resonance Reactions* (Oxford: Clarendon, 1968).

radioactive decay, the activity decays with time according to the total decay constant, even though we might observe only a single branch with a very different partial decay constant. The Γ^2 factor in the numerator, on the other hand, is directly related to the formation of the resonance and to its probability to decay into a particular exit channel. In the case of elastic scattering, for which Equation 11.65 was derived, the entrance and exit channels are identical. That is, for the reaction a + X → a + X, we should use the partial widths Γ_{aX} of the entrance and exit channels:

$$\sigma = \frac{\pi}{k^2} g \frac{(\Gamma_{aX})^2}{(E - E_R)^2 + \Gamma^2/4} \tag{11.69}$$

Similarly, for the reaction a + X → b + Y, a different exit width must be used:

$$\sigma = \frac{\pi}{k^2} g \frac{\Gamma_{aX}\Gamma_{bY}}{(E - E_R)^2 + \Gamma^2/4} \tag{11.70}$$

Equations 11.69 and 11.70 are examples of the *Breit-Wigner formula* for the shape of a single, isolated resonance. Figure 11.26 shows such a resonance with the Breit-Wigner shape. The cross section for resonant absorption of γ radiation has a similar shape, as given by Equations 10.29 and 10.30.

Many elastic scattering resonances have shapes slightly different from that suggested by the Breit-Wigner formula. This originates with another contribution to the reaction amplitude from direct scattering of the incident particle by the nuclear potential, without forming the resonant state. This alternative process is called *potential scattering* or *shape-elastic scattering*. Potential scattering and

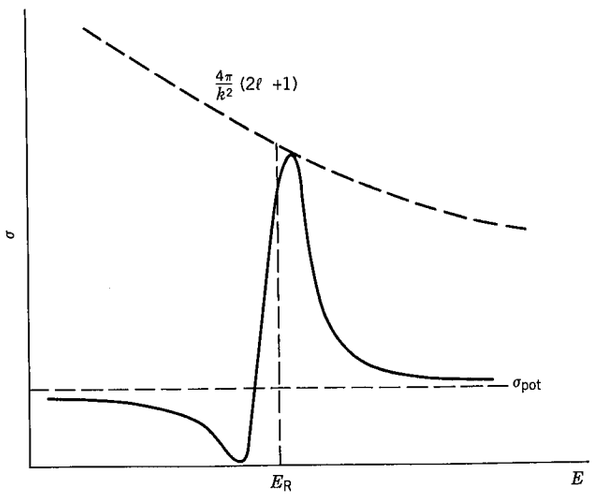

Figure 11.27 Interference between resonance and potential scattering produces resonances with this characteristic shape.

resonant scattering both contribute to the elastic scattering amplitude, and interference between the two processes causes variation in the cross section. Interference can cause the combined cross section to be smaller than it would be for either process alone. It is therefore not correct simply to add the cross sections for the two processes. We can account for the two processes by writing

$$\eta_\ell = e^{2i(\delta_{\ell R} + \delta_{\ell P})} \tag{11.71}$$

where $\delta_{\ell R}$ is the resonant phase shift, as in Equations 11.63 or 11.64, and $\delta_{\ell P}$ is an additional contribution to the phase shift from potential scattering. From

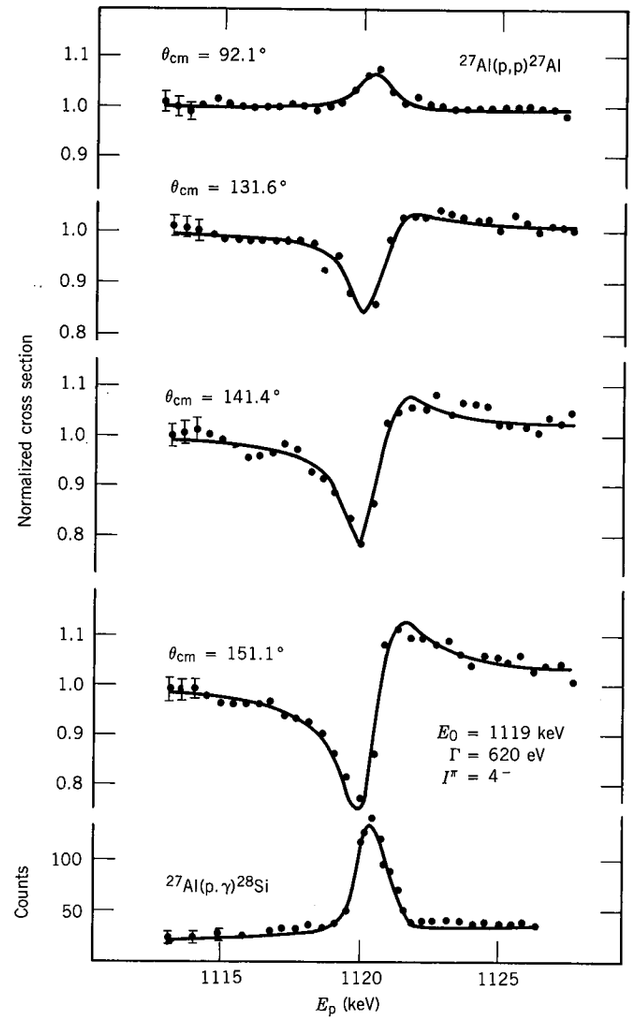

Figure 11.28 Resonances in the reaction ^{27}Al(p, p)^{27}Al. The resonances occur in the nucleus ^{28}Si. Note that the (p, γ) yield shows a resonance at the same energy. From A. Tveter, *Nucl. Phys. A* **185**, 433 (1972).

Equation 11.44 we find the cross section

$$\sigma_{sc} = \frac{\pi}{k^2}(2\ell+1)\left|e^{-2i\delta_{\ell P}} - 1 + \frac{i\Gamma}{(E-E_R)+i\Gamma/2}\right|^2 \qquad (11.72)$$

Far from the resonance, $(E - E_R) \gg \Gamma/2$ and the potential scattering term dominates:

$$\sigma \cong \sigma_{pot} = \frac{4\pi}{k^2}(2\ell+1)\sin^2\delta_{\ell P} \qquad (11.73)$$

At $E = E_R$, the resonant term dominates and

$$\sigma \cong \sigma_{res} = \frac{4\pi}{k^2}(2\ell+1) \qquad (11.74)$$

Near the resonance there is interference between the two terms, which produces the characteristic shape shown in Figure 11.27. According to this model, we

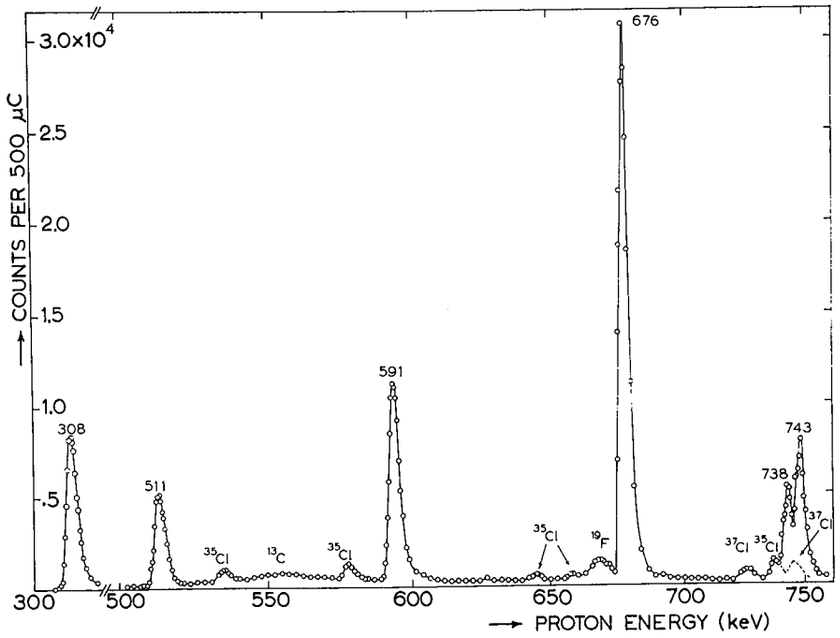

Figure 11.29 Resonances observed in the radiative proton capture by ^{23}Na. In this case, the total yield of γ rays in the energy range 3 – 13 MeV was measured as a function of the incident proton energy. The Cl peaks appear because the target used was NaCl. From P. W. M. Glaudemans and P. M. Endt, *Nucl. Phys.* **30**, 30 (1962).

expect an interference "dip" on the low-E side of the resonance. The resonance height should decrease roughly as k^{-2} (that is, as E^{-1}) with increasing incident energy, and the nonresonant "background" from potential scattering should remain roughly constant. Figure 11.28 shows scattering cross sections with the resonant structure clearly visible. The expectations of the resonance model are clearly fulfilled.

Radiative capture reactions also show a resonant structure. Figure 11.29 shows examples of (p, γ) reactions. Note that this is not a γ spectrum in the conventional sense—the horizontal axis shows the incident proton energy, not the emitted γ energy.

Resonances observed in neutron scattering are discussed in more detail in Chapter 12.

11.13 HEAVY-ION REACTIONS

From the point of view of nuclear reactions, a heavy ion is defined to be any projectile with $A > 4$. Accelerators devoted to the study of heavy-ion reactions can produce beams of ions up to ^{238}U, at typical energies of the order of 1–10 MeV per nucleon, although much higher energies are also possible.

The variety of processes than can occur in heavy-ion reactions is indicated schematically in Figure 11.30. At large impact parameters, Coulomb effects dominate, and Rutherford scattering or Coulomb excitation may occur. When the nuclear densities of the target and projectile just begin to overlap, nuclear reactions can occur, and at small overlap ordinary elastic or inelastic scattering and few-nucleon transfer through direct reactions may occur, as discussed previously in this chapter.

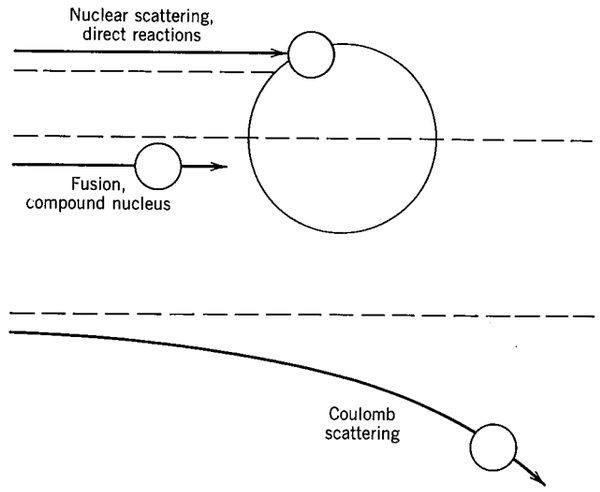

Figure 11.30 Processes in heavy-ion scattering depend on the impact parameter, when energies are large enough to penetrate the Coulomb barrier.

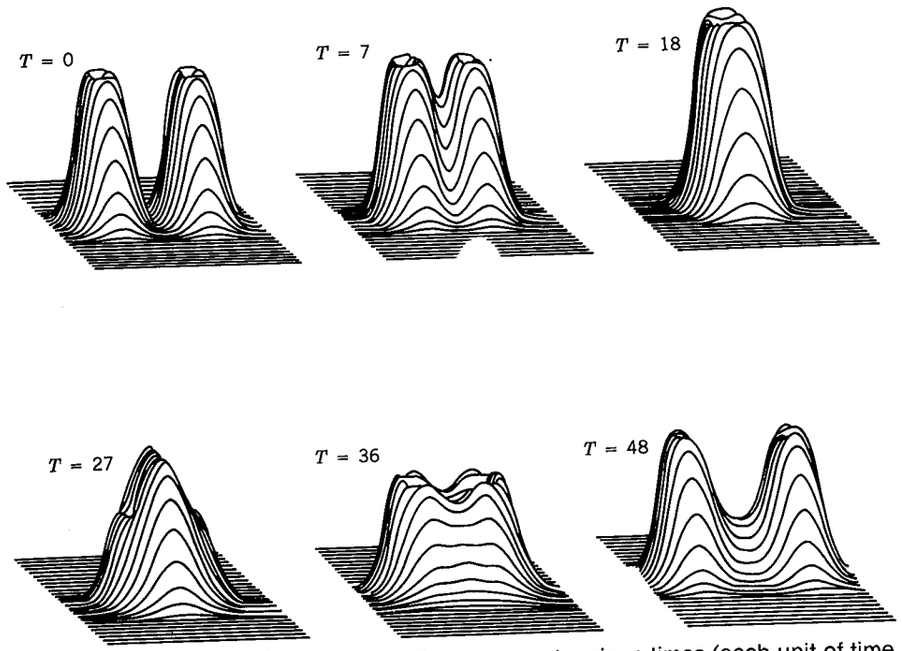

Figure 11.31 Two ^{12}C nuclei colliding, shown at various times (each unit of time is 3.3×10^{-24} s, and the area shown represents 1 fm^2). The vertical scale shows the nuclear density, which reaches a peak at $T = 11$. Note the internal oscillations that occur before the compound system breaks apart. The energy of the incident projectile was about 700 MeV. (Courtesy Ronald Y. Cusson and Joachim Maruhn, Oak Ridge National Laboratory; from *Scientific American*, p. 59, December 1978.)

At small impact parameters, new and unusual features emerge in these reactions. If the impact parameter is small enough that the nuclei can overlap completely, a compound nucleus, representing complete fusion of the two nuclei, can form as an intermediate state. However, to overcome the repulsive Coulomb barrier, the incident ion must be quite energetic, and thus the compound nucleus is formed with a considerable excitation energy. This compound nucleus may be an unusual state of nuclear matter that cannot be achieved in reactions with light nuclei. Because of the large incident energy, the compound nucleus may achieve a density or a "temperature" (that is, a mean internal kinetic energy per nucleon) beyond what can be achieved in reactions with light ions. The analysis of these compound states and their decay modes thus represent a challenge for nuclear theory—can we extrapolate from an equation of state for "ordinary" nuclear matter to one for "extraordinary" nuclear matter? Figure 11.31 shows an attempt to calculate the intermediate states through which the highly excited compound nucleus ^{24}Mg progresses in the course of the reaction $^{12}C + ^{12}C$.

Once the excited compound state is formed, there are many channels available for its decay. It can split more-or-less in half, either through the original entrance channel ($^{24}Mg \rightarrow ^{12}C + ^{12}C$) or through a closely related channel ($^{24}Mg \rightarrow ^{15}O + ^{9}Be$). For heavier nuclei, the study of the fission mode provides a check on theories derived from the study of the more familiar cases of transuranic fission, described in Chapter 13.

A more probable means of decay of the compound nucleus is through particle emission, for fission is inhibited by a substantial Coulomb barrier. Emission of charged particles (protons or α's) is also inhibited by a Coulomb barrier. In reactions with heavy nuclei the compound nucleus is extremely proton rich, but the preferred decay mode is still neutron emission; this remains so, even for heavy nuclei with a proton excess of 10–20 or more. It is thus possible to study nuclei far from stability on the proton-rich side through (HI, xn) reactions, where HI indicates any heavy ion and x may be in the range 5–10.

A particular application of these reactions is in the search for stable or nearly stable nuclei of *superheavy elements*. The transuranic atoms that have been studied through the neutron capture–β-decay technique move up the atomic number scale in single steps, but the technique loses its applicability for the nuclei around $Z = 104$ or 105, where the half-lives become very short ($\sim$ seconds) for decay by spontaneous fission. As Z increases, the spontaneous fission half-life should continue to decrease (because the Coulomb energy, which makes the nucleus more unstable to fission, increases like Z^2), until we approach the region of the next closed shell or "magic number" for protons, which has been calculated to be $Z = 114$ (rather than 126, as is already known for neutrons).

It is possible to search for superheavy nuclei directly, by bombarding the heaviest possible quasistable targets ($^{249}_{98}Cf$, with $t_{1/2} = 351$ y) with beams such as ^{32}S or ^{40}Ca, in the hope of producing stable products around $Z = 114$, $N = 164$ following few-nucleon emission from the compound state. Another possibility would be to produce a highly unstable, extremely heavy compound state in a reaction such as $^{238}U + ^{238}U$, in the hope that one of the fission decay channels would have a high probability of producing a stable superheavy nucleus. To date no success has been reported from either of these approaches, but the effort continues.

Another unique feature of heavy-ion reactions is the transfer of large amounts of angular momentum to the compound nucleus. For example, in the reaction

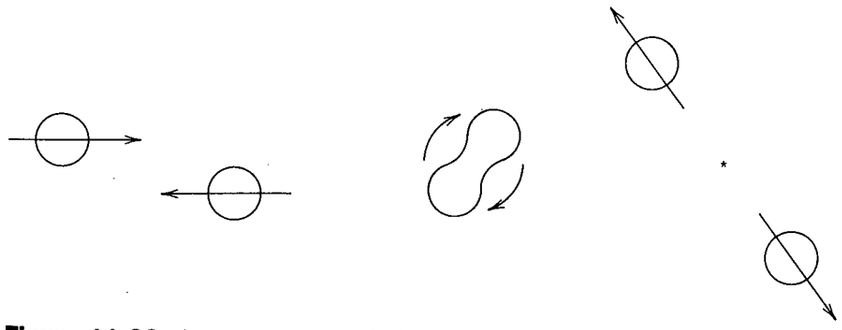

Figure 11.32 In nuclear molecule formation, there is not quite complete fusion of the two particles; they retain a "memory" of their previous character and break apart accordingly. The internal energy of the system can show rotational and vibrational structures, just like an ordinary molecule.

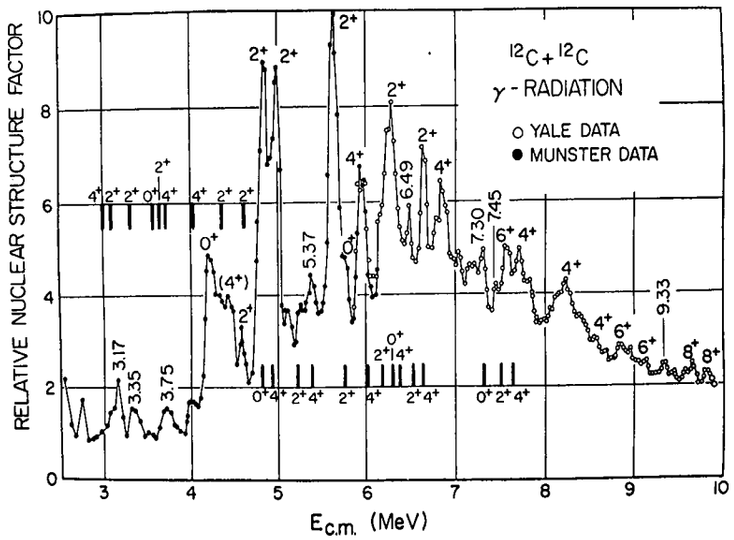

(a)

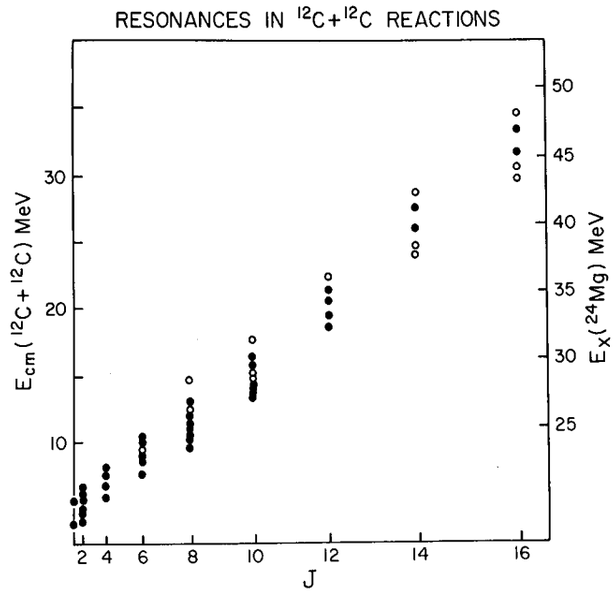

(b)

Figure 11.33 (*a*) The $^{12}C + ^{12}C$ molecular states. The vertical scale shows the cross section with the "uninteresting" Coulomb penetrability factor removed, leaving the nuclear structure factor. The resonances are labeled with the spin-parity assignments which can be grouped into rotational sequences $0^+, 2^+, 4^+, 6^+, \ldots$. (*b*) Plotting the internal excitation energies of the resonances against $I(I+1)$ reveals that the states do indeed form rotational sequences. From T. M. Cormier, *Ann. Rev. Nucl. Particle Sci.* **32**, 271 (1982).

$^{40}Ca + ^{197}Au$, the Coulomb barrier is about 200 MeV. If we use 200 MeV incident ^{40}Ca, a grazing collision will provide about $140\hbar$ of angular momentum to the system. Even at collisions with smaller impact parameters, it would not be unusual to transfer an angular momentum of $\ell \gtrsim 40\hbar$ to the compound system. At such rotational velocities, the nuclear force may not be able to provide the necessary centripetal acceleration, and the compound system may be completely unstable and therefore unable to form. In such a case, a new type of system is possible, called a *nuclear molecule*. Figure 11.32 illustrates the process schematically. The two nuclei do not form a compound system, corresponding to complete sharing of the incident energy. Instead a system analogous to a diatomic molecule is formed, exists for a short time, and then breaks apart in the same configuration as the incident particles. Because the decay occurs into the original particles, the combined system retains a considerable "memory" of its formation, contrary to the basic assumption of the compound-nucleus model. Evidence for such molecular states comes from observing the rotational and vibrational excitations that correspond closely with those observed in ordinary molecules. Figure 11.33 shows an example of the states observed in the $^{12}C + ^{12}C$ nuclear molecule. Resonances in the cross section correspond to the rotational and vibrational states permitted in the molecular system.

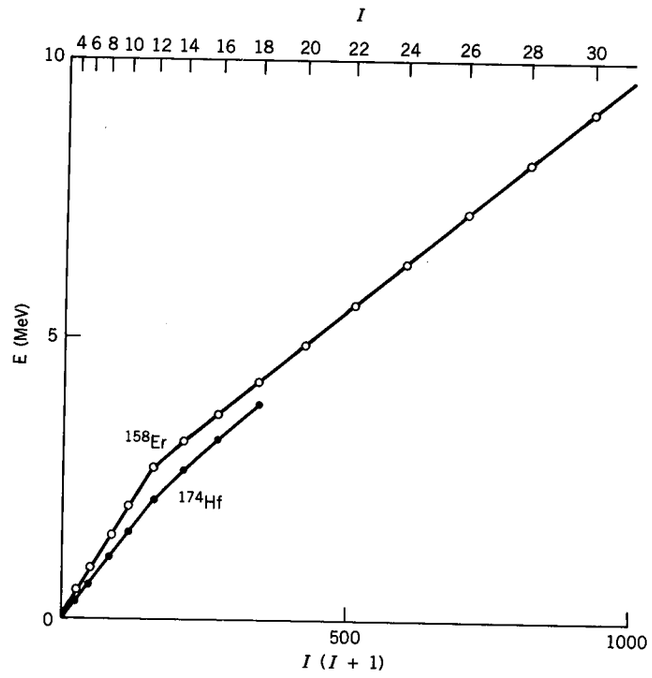

Figure 11.34 Rotational energies of ^{158}Er and ^{174}Hf. Neither case shows the expected linear dependence of E on $I(I+1)$, but in ^{174}Hf the deviation is relatively gradual, while in ^{158}Er there appears to be a sudden change in slope (and therefore in moment of inertia) in the neighborhood of $I = 12-14$.

In heavier nuclei, highly excited states with $\ell \gtrsim 40$–$50\hbar$ can be populated in the compound system. The emission of a few neutrons from the excited system can change the angular momentum only little (a 5-MeV neutron carries at most only $\ell \sim 3\hbar$), and following the neutron emission, excited bound states in the final nucleus can be formed with angular momentum quantum numbers of 40 or so. Assuming the product nucleus to be of the deformed even-Z, even-N variety, the excited states will show a rotational spectrum of the type illustrated in Figure 5.22. The rotational energies are given by Equation 5.17:

$$E = \frac{\hbar^2}{2\mathscr{I}} I(I+1) \tag{11.75}$$

and the states should cascade down toward the ground state through a sequence of $E2$ γ transitions as in Figure 10.18. The observation of these cascade $E2$ transitions provides a way to study these excited states. In particular, we can study whether the assumption of a fixed, constant moment of inertia $\mathscr{I}$ remains valid at such high excitations. One way to test this assumption is to plot the energies of the states against $I(I+1)$ and to see if the slope remains constant, as predicted by Equation 11.75. Figure 11.34 is an example of such a plot, and there appears to be some deviation from the expected linear behavior.

There is a more instructive way to plot the data on the rotational structure. From Equation 11.75, the energy of a transition from state I to the next lower state $I-2$ is

$$E(I) - E(I-2) = \frac{\hbar^2}{2\mathscr{I}}(4I-2) \tag{11.76}$$

The transition energies should increase linearly with I; Figure 11.35 shows that this is true for the lower transitions, but becomes less valid as we go to larger I, and in fact the behavior changes completely at about $I = 16$, but then seems to restore itself as we go to higher states.

Let's assume that the moment of inertia is not constant, but increases gradually as we go to more rapidly rotating states; this effect, known classically as "centrifugal stretching," would not occur for a rigid rotor but would occur for a fluid. Because rotating nuclei have moments of inertia somewhere between that of a rigid rotor and of a fluid, as described in Equations 5.18 and 5.19, it is not surprising that centrifugal stretching occurs. Representing the rotational energy in terms of the rotational frequency

$$E = \tfrac{1}{2}\mathscr{I}\omega^2 \tag{11.77}$$

we can then assume $\mathscr{I}$ varies either with increasing angular momentum,

$$\mathscr{I} = \mathscr{I}_0 + kI(I+1) \tag{11.78}$$

or with increasing rotational frequency,

$$\mathscr{I} = \mathscr{I}_0 + k'\omega^2 \tag{11.79}$$

where k and k' are appropriate proportionality constants. From Equation 11.76,

$$\frac{2\mathscr{I}}{\hbar^2} = \frac{4I-2}{E(I)-E(I-2)} \tag{11.80}$$

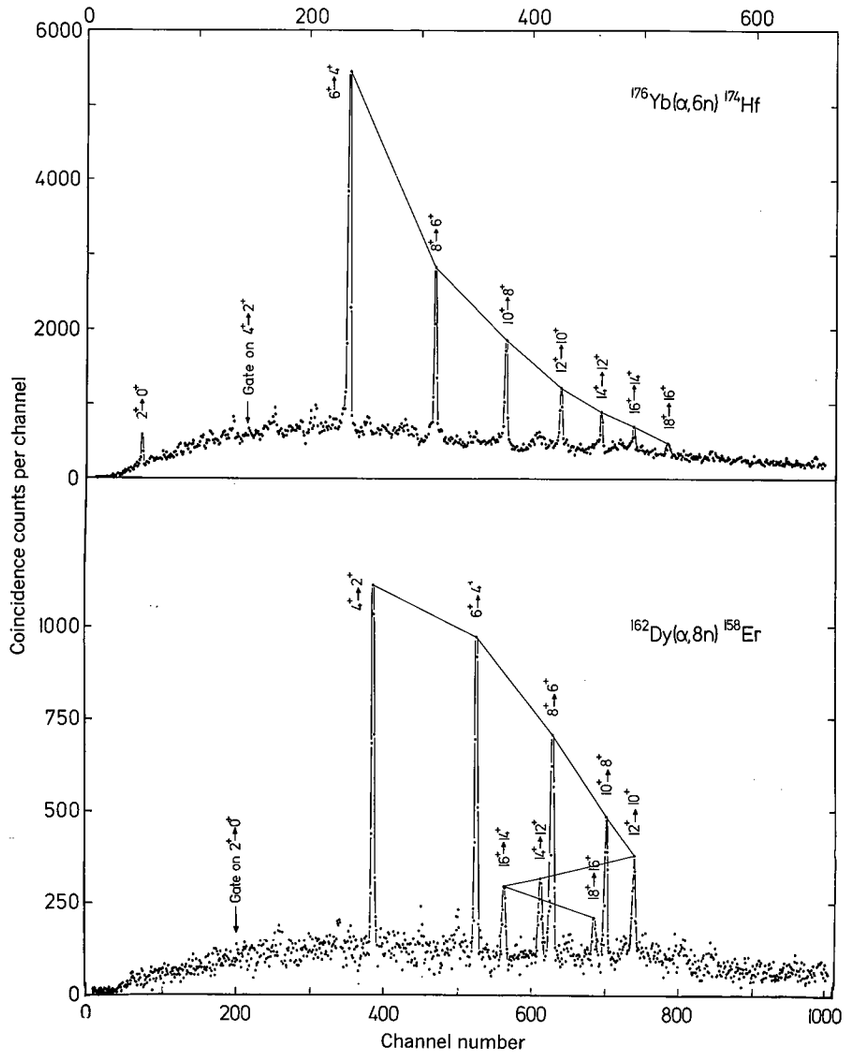

Figure 11.35 γ-ray spectra of transitions between rotational states in ^{158}Er and ^{174}Hf. For a perfect rotor, the γ-ray energies should increase monotonically with I. This is so for ^{174}Hf, but for ^{158}Er the energy begins to *decrease* with I in the range $I = 12-16$, and after $I = 16$ the energy again begins to increase. From R. M. Lieder and H. Ryde, in *Advances in Nuclear Physics*, Vol. 10, edited by M. Baranger and E. Vogt (New York: Plenum, 1978).

and plotting $\mathscr{I}$, measured in these units, against ω^2, we ought to see either a constant $\mathscr{I}_0$ if no stretching occurs, or a linear behavior. Figure 11.36 shows an example of such a relationship. There appears to be a gradual increase in $\mathscr{I}$ among the lower angular momentum states, then a radical change in behavior around $I = 16$, and then a return to the gradual stretching. This effect is known as *backbending*, and occurs because the rotational energy exceeds the energy

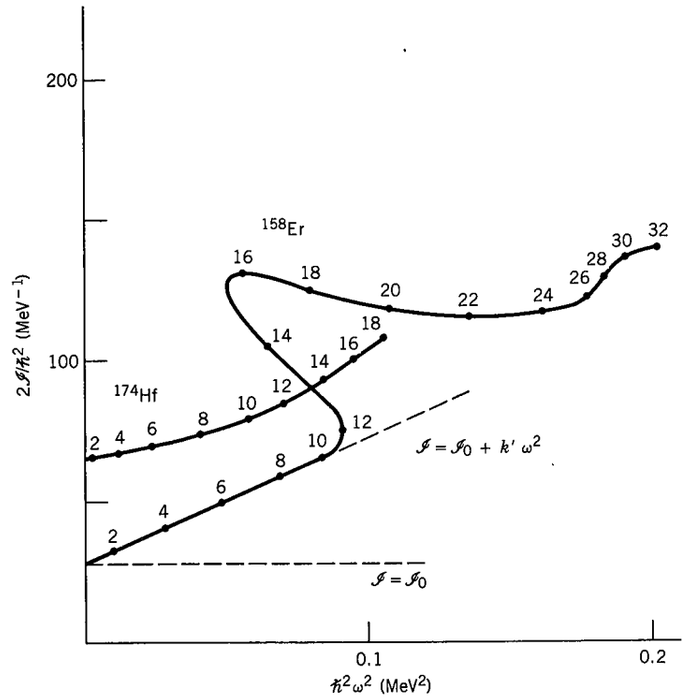

Figure 11.36 Moment of inertia, from Equation 11.80, as a function of $\hbar^2\omega^2$, from the semiclassical formula $\frac{1}{4}[E(I) - E(I-2)]^2$. Note the gradual increase in the moment of inertia for the lower states in both ^{158}Er and ^{174}Hf, and note also the backbending in ^{158}Er.

needed to break a pair of coupled nucleons. When that occurs (at an energy corresponding to $I = 16$), the unpaired nucleons go into different orbits and change the nuclear moment of inertia. The situation then remains stable until about $I = 30$, where another pair is broken and another change in moment of inertia occurs.

The study of the properties of nuclei at high angular momentum is another example of an unusual state of nuclear matter accessible only through heavy-ion reactions.

A final example of the nuclear structure studies that can be done through heavy-ion reactions is the α-particle transfer reaction, such as (^{16}O, ^{12}C). In our discussion of α decay in Chapter 8, we alluded to the "preformation" of the α particle inside the nucleus. Because the α particle is such a stable structure, we can consider the nucleons in a nucleus to have a high probability of occasionally forming an α particle, even in nuclei that do not α decay. This leads to the *α-cluster* model of nuclei, in which we look for nuclear structure characteristic of such clusters. States populated in (^{16}O, ^{12}C) reactions, in which four nucleons are simultaneously transferred to the target nucleus, might be analyzed in terms of the transfer of an α cluster from ^{16}O to the target. Figure 11.37 illustrates the cross sections for the formation of states in ^{20}Ne through α-transfer reactions.

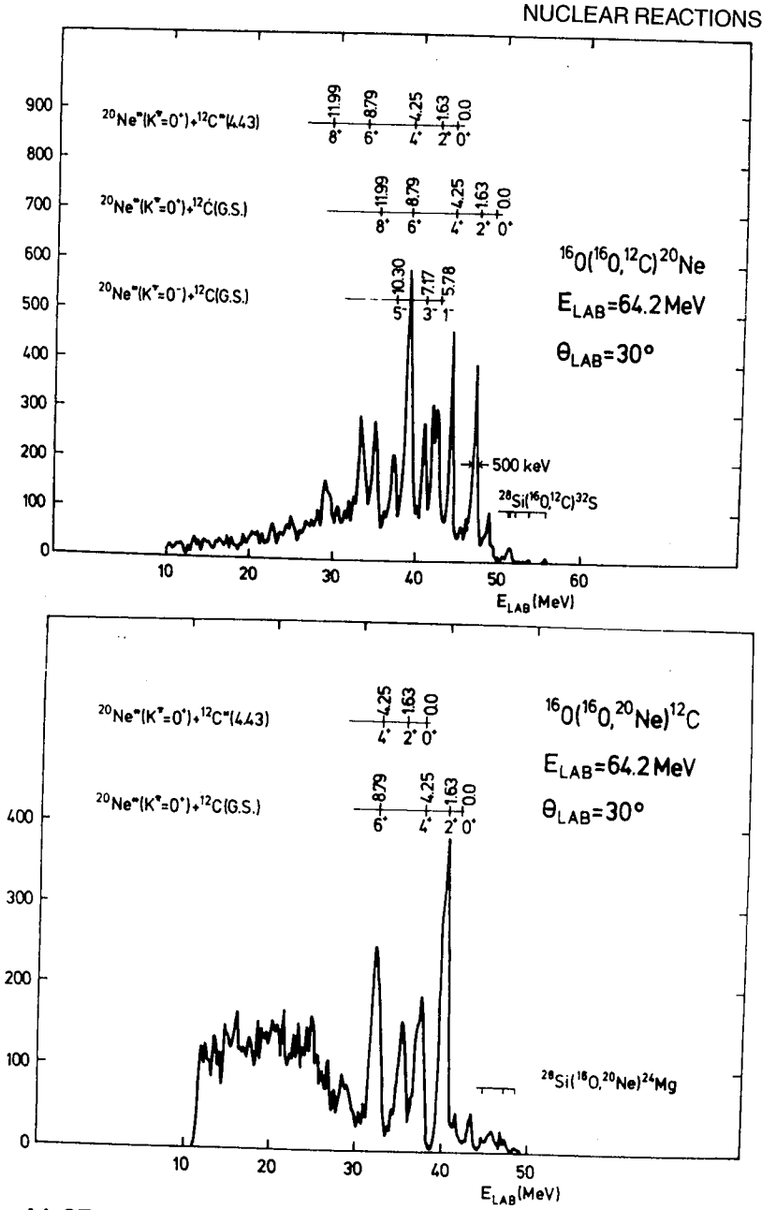

Figure 11.37 α-particle transfer reactions leading to ^{20}Ne. At top is the observed ^{12}C spectrum and at bottom is the ^{20}Ne spectrum. Individual excited states in ^{20}Ne are labeled, with some peaks in the spectrum assigned to reactions in which ^{12}C is left in its first excited state at 4.43 MeV. On the following page are shown the excited states of ^{20}Ne. Notice the selectivity of the reaction in populating certain states and not others; the dashed lines show states that are not populated in the reaction. Because the ^{16}O projectile and target are doubly closed-shell nuclei ($Z = 8, N = 8$), the observed states in ^{20}Ne correspond to the addition of an α particle to a doubly magic core; that is, the four valence nucleons are coupled to a resultant spin of zero, but can carry a net orbital angular momentum. Only a small subset of the ^{20}Ne states will have this character. Data from H. H. Rossner et al., *Nucl. Phys. A* **218**, 606 (1974).

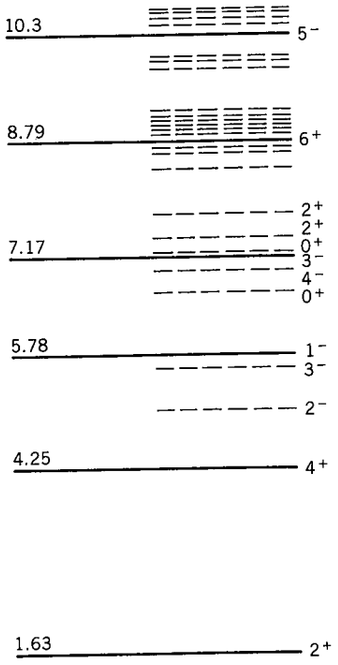

Figure 11.37 Continued.

REFERENCES FOR ADDITIONAL READING

A more complete description of nuclear reactions, at about the same level as this chapter, is by G. R. Satchler, *Introduction to Nuclear Reactions* (New York: Wiley, 1980). A reference at a similar level is I. E. McCarthy, *Nuclear Reactions* (Oxford: Pergamon, 1966). A more advanced text is P. E. Hodgson, *Nuclear Reactions and Nuclear Structure* (Oxford: Clarendon, 1971).

The most comprehensive recent review of all aspects of nuclear reactions is the four-part collection, *Nuclear Spectroscopy and Reactions*, edited by Joseph Cerny (New York: Academic, 1974). It includes chapters on direct reactions, resonance reactions, scattering, Coulomb excitation, and heavy-ion reactions, as well as material on experimental techniques.

Comprehensive summaries of the role of isospin in nuclear decays and reactions can be found in *Isospin in Nuclear Physics*, edited by D. H. Wilkinson (Amsterdam: North-Holland, 1969). Wilkinson's introduction is highly recommended as a review of the historical development of isospin and of nuclear theory.

Effects at high rotational velocities are discussed by R. M. Lieder and H. Ryde, in *Advances in Nuclear Physics*, Vol. 10, edited by M. Baranger and E. Vogt (New York: Plenum, 1978); see also the brief review by R. M. Diamond and F. S. Stephens, *Nature* **310**, 457 (1984).

PROBLEMS

1. Complete the following reactions:

$$^{27}\mathrm{Al} + \mathrm{p} \rightarrow \quad + \mathrm{n}$$
$$^{32}\mathrm{S} + \alpha \rightarrow \quad + \gamma$$
$$^{197}\mathrm{Au} + ^{12}\mathrm{C} \rightarrow ^{206}\mathrm{At} +$$
$$^{116}\mathrm{Sn} + \quad \rightarrow ^{117}\mathrm{Sn} + \mathrm{p}$$

2. (a) Solve Equations 11.3 and 11.4 for $\cos\theta$. (b) Determine the relationship between $\cos\theta$ and p_b for elastic scattering. (c) Show that there is a maximum value of θ only when $m_a > m_Y$. (d) Find the maximum angle at which α particles appear after elastic scattering from hydrogen and from deuterium.

3. It is desired to study the first excited state of $^{16}\mathrm{O}$, which is at an energy of 6.049 MeV. (a) Using the (α, n) reaction on a target of $^{13}\mathrm{C}$, what is the minimum energy of incident alphas which will populate the excited state? (b) In what direction will the resulting neutrons travel? (c) If it is desired to detect the neutrons at 90° to the incident beam, what is the minimum α energy that can result in the excited state being populated?

4. (a) In Coulomb scattering of 7.50-MeV protons by a target of $^{7}\mathrm{Li}$, what is the energy of the elastically scattered protons at 90°? (b) What is the energy of the inelastically scattered protons at 90° when the $^{7}\mathrm{Li}$ is left in its first excited state (0.477 MeV)?

5. The (n, p) reaction can be regarded as equivalent to β^+ decay in that the same initial and final nuclei are involved. Derive a general expression relating the Q value of the (n, p) reaction to the maximum energy release in β^+ decay. Find several examples to verify your derived relationship.

6. The Q value for the reaction $^{9}\mathrm{Be}(\mathrm{p}, \mathrm{d})^{8}\mathrm{Be}$ is 559.5 ± 0.4 keV. Use this value along with the accurately known masses of $^{9}\mathrm{Be}$, $^{2}\mathrm{H}$, and $^{1}\mathrm{H}$ to find the mass of $^{8}\mathrm{Be}$.

7. (a) Calculate the Q value of the reaction $\mathrm{p} + ^{4}\mathrm{He} \rightarrow ^{2}\mathrm{H} + ^{3}\mathrm{He}$. (b) What is the threshold energy for protons incident on He? For α's incident on hydrogen?

8. For the reaction $^{2}\mathrm{H} + ^{2}\mathrm{H} \rightarrow ^{3}\mathrm{He} + \mathrm{n}$, plot the energy of the outgoing neutron as a function of angle for $^{2}\mathrm{H}$ incident on $^{2}\mathrm{H}$ at rest. Use incident energies of 0.00, 2.50, and 5.00 MeV.

9. Compute the Q values for the reactions (a) $^{6}\mathrm{Li} + \mathrm{p} \rightarrow ^{3}\mathrm{He} + ^{4}\mathrm{He}$; (b) $^{59}\mathrm{Co} + \mathrm{p} \rightarrow \mathrm{n} + ^{59}\mathrm{Ni}$; (c) $^{40}\mathrm{Ca} + \alpha \rightarrow \mathrm{n} + ^{43}\mathrm{Ti}$.

10. For the following endoergic reactions, find the Q value and the threshold kinetic energy, assuming in each case that the lighter particle is incident on the heavier particle at rest: (a) $^{7}\mathrm{Li} + \mathrm{p} \rightarrow ^{7}\mathrm{Be} + \mathrm{n}$; (b) $^{12}\mathrm{C} + \mathrm{p} \rightarrow \mathrm{n} + ^{12}\mathrm{N}$; (c) $^{35}\mathrm{Cl} + \alpha \rightarrow \mathrm{n} + ^{38}\mathrm{K}$.

11. At threshold, the product particles Y + b move at the same velocity. Use momentum conservation to derive a relationship between T_a and T_b at threshold, and then substitute your expression into Equation 11.5 to obtain the threshold condition (11.6).

12. It is desired to study the low-lying excited states of ^{35}Cl (1.219, 1.763, 2.646, 2.694, 3.003, 3.163 MeV) through the $^{32}S(\alpha, p)$ reaction. (a) With incident α particles of 5.000 MeV, which of these excited states can be reached? (b) Again with 5.000-MeV incident α's, find the proton energies observed at 0, 45, and 90°.

13. In the reaction $^{7}Li + p \rightarrow {}^{4}He + {}^{4}He$ (18.6 MeV protons incident on a lithium target) the differential cross section (in the center-of-mass system) reaches a maximum of about 1.67 barns/steradian at a center-of-mass angle of 75°. (a) Sketch the reaction kinematics in the laboratory system, labeling all momenta, directions, and energies. (b) Assuming a target thickness of 1.0 mg/cm^2 and a beam of protons of current 1.0 μA spread over an area of 1 cm^2, find the number of α particles per second in the above geometry that would strike a detector of area 0.5 cm^2 located 12.0 cm from the target.

14. The radioactive isotope ^{15}O, which has important medical applications (see Chapter 20), can be produced in the reaction $^{12}C(\alpha, n)$. (a) The cross section reaches a peak when the laboratory energy of the incident α particles is 14.6 MeV. What is the excitation energy of the compound nuclear state? (b) The reaction cross section at the above incident energy is 25 mb. Assuming a carbon target of 0.10 mg/cm^2 and a current of 20 nA of α's, compute the ^{15}O activity that results after 4.0 min of irradiation.

15. In a Coulomb excitation experiment, α particles are inelastically scattered from ^{160}Dy nuclei. (a) If the incident energy is 5.600 MeV, what is the energy of the elastically scattered α's observed at $\theta = 150°$? (b) States in ^{160}Dy are known at 2^+(0.087 MeV), 4^+(0.284 MeV), and 2^+(0.966 MeV). Considering only the $E2$ excitation mode, find the energies of the inelastically scattered α's observed at 150°.

16. What should be the incident energy of a beam of protons to be Coulomb scattered by gold nuclei, if it is desired that the minimum distance between projectile and target should correspond to the two nuclei just touching at their surfaces?

17. Alpha particles of energy 8.0 MeV are incident at a rate of 3.0×10^7 per second on a gold foil of thickness 4.0×10^{-6} m. A detector in the form of an annular ring is placed 3.0 cm from the scattering foil and concentric with the beam direction; the annulus has an inner radius of 0.50 cm and an outer radius of 0.70 cm. What is the rate at which scattered particles strike the detector?

18. Alpha particles of energy 6.50 MeV are Coulomb scattered by a gold foil. (a) What is the impact parameter when the scattered particles are observed at 90°? (b) Again for scattering at 90°, find the smallest distance between the α particles and the nucleus, and also find the kinetic and potential energies of the α particle at that distance.

19. Protons of energy 4.00 MeV are Coulomb scattered by a silver foil of thickness 4.0×10^{-6} m. What fraction of the incident protons is scattered at angles (a) beyond 90°? (b) Less than 10°? (c) Between 5 and 10°?

20. Derive Equations 11.49–11.51 for "black disk" scattering.

21. Give the compound nucleus resulting from protons bombarding an aluminum target, and give at least five different ways for the compound nucleus to decay.

22. For the states of ^{61}Cu populated in the (α, p) reaction, Figure 11.4, find the ℓ transfer for each of the states.

23. In the (d, p) reaction leading to states in ^{91}Zr, as shown in Figures 11.23 and 11.24, discuss the possible final angular momentum states if the reaction could proceed by a compound-nucleus mechanism. As an example, consider whether it still is possible to associate a final $I^\pi = \frac{7}{2}^+$ state uniquely with $\ell = 4$. Discuss other final states as well.

24. The low-lying levels of ^{43}Sc were illustrated in Figure 5.12. It is desired to populate the states up to the $\frac{7}{2}^-$ excited state with the (d, n) reaction. Estimate the most likely angle for the outgoing neutrons for each excited state. (Try to estimate the excited-state energies from the figure.)

25. The (d, p) reaction on ^{49}Ti ($\frac{7}{2}^-$ ground state) populates the "collective" 0^+, 2^+, and 4^+ states at 0.000, 1.555, and 2.675 MeV (respectively) in ^{50}Ti. What are the angular momentum values transferred in the direct reaction?

26. The (^{3}He, p) reaction on an even-Z, even-N target leads to certain final states identified with the transfer of either $\ell = 0$, 2, or 4. (a) For each choice, list the possible spin-parity assignments in the final nucleus. (b) In some cases, the analysis suggests that certain states are populated by a mixture of $\ell = 0$ and $\ell = 2$, while others are populated by a mixture of $\ell = 2$ and $\ell = 4$. Is it possible to make a unique determination of the final spin in either of these cases?

27. The (d, p) reaction on ^{52}Cr leads to the $\frac{3}{2}^-$ ground state of ^{53}Cr. How would the analysis of the angular momentum transfer in this reaction differ between an analysis in terms of direct reactions and one in terms of compound-nucleus reactions?